STRUCTURAL LOCKING IN A NASTIC ACTUATED SHAPED-CHANGING BEAM

A Thesis

by

GENE CHA

Submitted to the Office of Graduate Studies of
Texas A&M University
in partial fulfillment of the requirements for the degree of

MASTER OF SCIENCE

May 2010

Major Subject: Mechanical Engineering

STRUCTURAL LOCKING IN A NASTIC ACTUATED SHAPED-CHANGING BEAM

A Thesis

by

GENE CHA

Submitted to the Office of Graduate Studies of
Texas A&M University
in partial fulfillment of the requirements for the degree of

MASTER OF SCIENCE

Approved by:

Chair of Committee,	Terry S. Creasy
Committee Members,	Ibrahim Karaman
	Wayne N.P. Hung
Head of Department,	Dennis L. O'Neal

May 2010

Major Subject: Mechanical Engineering

ABSTRACT

Structural Locking in a Nastic Actuated Shaped-Changing Beam.

(May 2010)

Gene Cha, B.S., Kyung Hee University

Chair of Advisory Committee: Dr. Terry S. Creasy

This thesis endeavors to develop a new locking method for a twisted morphing wing spar. The conventional wing has to have hinges and a discontinuous surface. These cause air separation that decreases aerodynamic performance. Unlike this old concept, the new airfoil comprises a square cross section spar into the wing blade. Twisting the spar changes the airfoil's angle of attack to control lifting and thrust force without a discontinuous surface.

A nastic actuator generates shear stress for twisting the spar. A thermoplastic polymer locks the twisted shape. Applying heat and solidifying the polymer makes the beam lock into the twisted position even after removing the shear stress. This concept was evaluated by computer simulation and an experiment with a prototype construction.

The analysis with 5m long spar shows that $\pm$450Pa shear stress generated $\pm$2 degrees twist and maximum 1.49MN/m spring constant at the spar tip. This spring constant helps a designer select the locking material, Ultem. The analysis proves that the Ultem film's shear spring constant is high enough to hold the aluminum spar's spring back.

Physical experiment conditions might differ from computer simulation because environmental limitations might be present. The prototype spar has to be less than 300mm long to fit in an electric oven. Tension made the beam twist and baked it with locking material. When the polymer softened, the beam was taken from the oven and cooled. The solidified locking material held the spar at twisted status. The observation shows no detectable spring back after removing tension. Analytic solution also presents no spring back in twisting the prototype section spar. The FEA of the section spar verifies the physical experiment results.

As a normal polymer, the Ultem shows stress relaxation. The load drop affects deceasing elastic modulus. Subsequently, the Ultem is able to lock the twisted spar even after the relaxation.

DEDICATION

To my parents and my great brother

ACKNOWLEDGEMENTS

I would like to thank my advisor and committee chair, Dr. Creasy for his guidance and support, and my committee members, Dr. Karaman, and Dr. Hung throughout this research.

I also want to extend my gratitude to the Defense Advanced Research Projects Agency (DARPA) that provided the fund for this work based upon work supported by DARPA and the US Army Research, Development and Engineering Command.

This material is based upon work supported by the US Army Research, Development and Engineering command under contract number W911W6-05-C-0015. Any opinions, findings, and conclusions or recommendations expressed in this material are those of the author(s) and do not necessarily reflect the views of the US Army Research, Development and Engineering Command.

I also would like to express appreciation to my colleagues, Sang Jin Lee, Jaehyeuk Jeon, Roston Elwell, and Viral Shah for their helps.

Finally, thanks to my mother, Dr. Si Ja Chun, father, Dr. Cheol Ho Cha, and my great brother, Joseph H. Cha for their encouragement.

TABLE OF CONTENTS

Page

Page

LIST OF FIGURES

Page

Page

Page

Page

Page

1. INTRODUCTION

1.1 Overview and Motivation

Shape changing structures in nature are efficient. The human body has many degrees-of-freedom, and a plant like the Venus flytrap generates large strain in a short time. Manufactured structures achieve shape changes with inefficient, cumbersome actuators and hinges that have limited degrees-of-freedom. If advanced materials can accommodate shape-changing functions, the overall structure might be more efficient.

Sater and Main suggested nastic materials that mimic specific plants' movement might provide multifunctional structures [1]. Some plants, like the ‘trigger plant’ Stylidium, produce large strains in a short time. The Stylidium’s fused male/female reproductive column responds to touch as shown in Figure 1. When a pollinating insect lands on its flower, turgor pressure produces a physiological change that rapidly sends the column, which showers the insect with pollen, toward the insect [2]. Although Stylidium deploys this action rapidly and resets it slowly, synthetic nastic materials might be possible with actuation rates that can vary from rapid, large motions to slow, small movements.

These new material concepts are most effective in high performance applications, and aerospace structures are high performance designs. A good candidate for the nastic materials is the wing because even simple wings require shape changes to expand the

---

This thesis follows the style of *AIAA JOURNAL*.

flight envelope from slow speeds for takeoffs and landings to an efficient shape for long duration flights. When embedded throughout the structure, these active materials might replace complex mechanical joints and control the wing shape effectively. One challenge in developing morphing wings is maintaining their structural stiffness or aeroelasticity while changing their shape [3]. The wings must be stiff to keep their shape under aeroelastic loads and to avoid flutter. However, high stiffness inhibits shape changing for landing and takeoff.

Figure 1. These Stylidium photographs show the flower with its reproductive column ready to snap forward in the left image and with the column moved forward in the right image [4].

1.2 Objective

This thesis presents a method for locking the split spar proposed by Hawkins et al. for application in a variable-twist wing spar [5]. For this study, a generic, cantilever

wing beam presents the structural challenges for variable twist; however, the generic wing has no specific aerodynamic shape or application. Figure 2 shows that, as in a wing, a square spar stiffens the beam in bending and the spar and outer skin resist torsion around the beam's long axis. This generic wing has a split spar. One side splits along the longitudinal axis; this split opens the cross section and lowers its torsional resistance. A high-stiffness thermoplastic polymer strip fills the gap to make the spar a torsionally stiff, closed section whenever the polymer bonds the flanges together. The permanently open cross-section beam is not appropriate for the main structure because its torsional rigidity is low, but the polymer strip must close the cross section to satisfy aeroelasticity. In this thesis, the polymer is the locking material. This project's objective is to find the polymer material properties required to provide torsional stiffness as the polymer locks a demonstration spar in untwisted and twisted states.

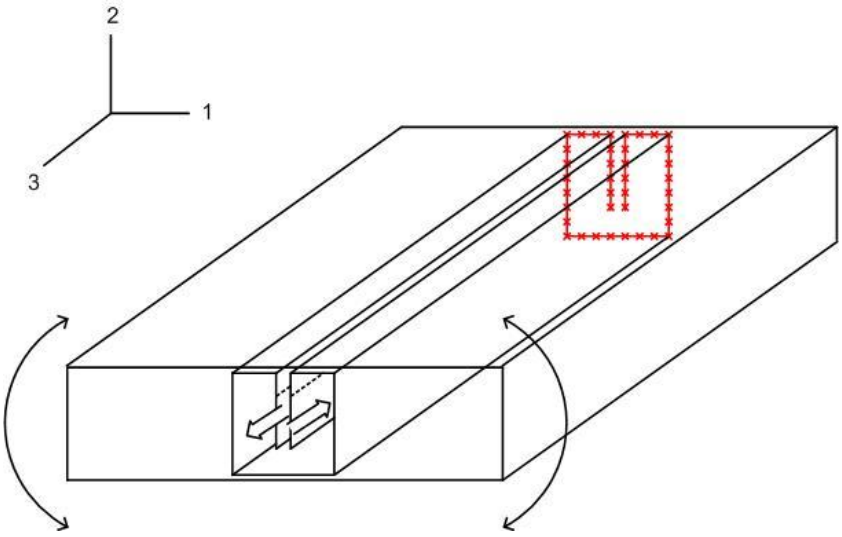

Figure 2. This generic wing has a split spar. One side splits along the longitudinal axis, and this split opens the cross section and lowers its torsional resistance. The root end is a clamped condition. The other tip end is free, and shows twist.

1.3 Scope

This thesis focuses on a new cyclic locking method for a twisted spar driven by nastic actuators. This concept has applications for wings as well as for other shape changing structures driven by smart materials. The work followed this plan:

1. Design an open spar that forms a closed spar when bonded.

2. Use Finite Element Analysis (FEA) to find the nastic material action necessary to twist the spar.

3. Use FEA to find the stiffness needed in a thermoplastic polymer that can lock the spar into a closed structure.

4. Validate the model with experiments using an example polymer.

2. PREVIOUS WORK

2.1 Primitive Shape-Changing Wings

Conventional aircraft have mechanical joints and hinges that connect the wing's components to control their positions and adjust the wing's shape. The F-111 Aardvark in Figure 3 needs extra joints for variable sweep wings. When the vehicle takes off and lands, the wings unfold for efficient low speed flight. For high speed, the wings sweep back and reduce the drag force.

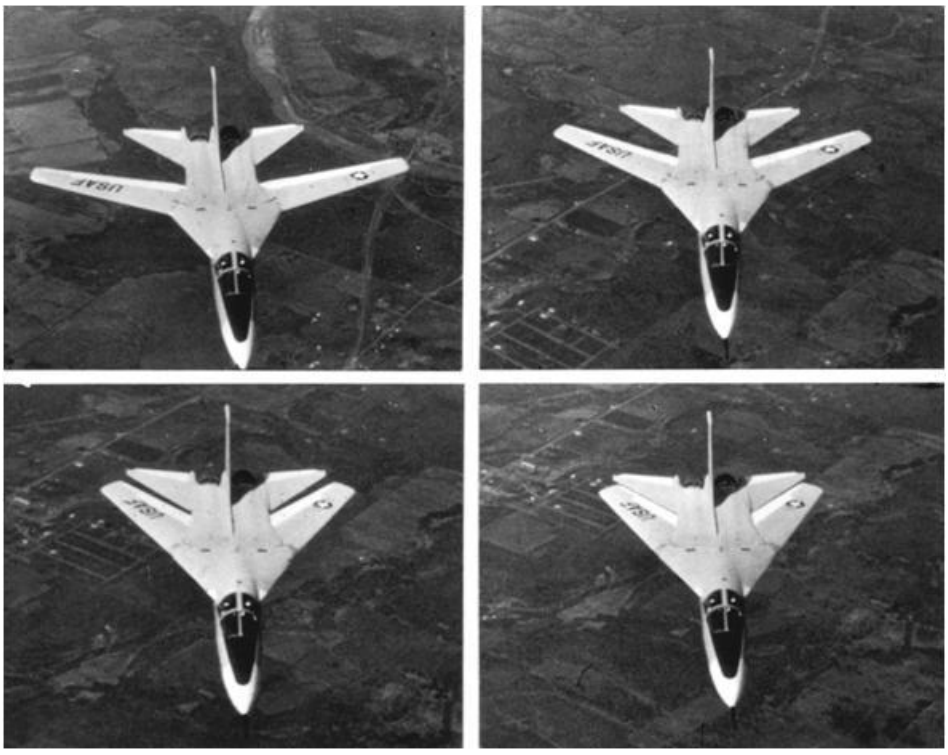

Figure 3. F-111 Aardvark with variable sweep wings [6].

However, this rigid structure adjustment makes the wings and fuselage discontinuous, and discontinuities disturb the airflow. The result is decreased lift and increased drag [7]. In addition, this structure has few degrees-of-freedom—it can perform well under two conditions: takeoff/landing and supersonic dash. For more degrees-of-freedom, the wing needs more mechanical joints and those joints increase weight [8].

2.2 Advanced Morphing Wing Goals

Morphing wings promote efficiency by replacing hinges and mechanical joints to reduce air separations and by reducing weight. Continuous wing surface control allows more DOF than conventional wings and reduces or eliminates hinges and joints. Davidson et al.'s[9] Hyper-Elliptic Cambered Span (HECS) concept vehicle has morphable wings. Depending on immediate need, the wing shape transforms into a drag tip, lift tip, or baseline geometry. The Mission Adaptive Compliant Wing (MACW) [10] in Figure 4 shows another morphing wing example. The wing's shape is like Figure 4 (a) during cruising, and the wing transforms for landing or takeoff as shown in Figure 4 (b).

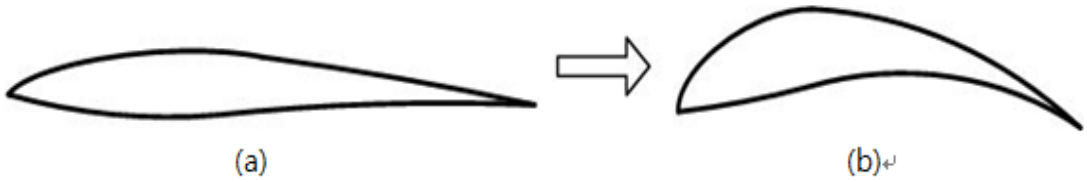

Figure 4. Morphing aircraft wings transform their shape in response to changing flight condition (Redrawn from [10]).

Rather than replace the conventional actuator-hinge-joint structure with internalized discrete actuators with the same weight penalties, current research focuses on active materials that affect shape changes when they receive energy to drive the change. The next section reviews active material development.

2.3 Active Materials for Morphing Structures

Active materials are substances that incorporate an actuator within their structure. They can perform work when provided with energy, which can be mechanical, electrical, or chemical. Their performance characteristics are force, displacement, density, modulus, power, and efficiency. It is essential to understand those characteristics when choosing an active material [8]. Conventional aircraft use hydraulic actuators when changing their wing shapes. Figure 5 shows several active materials and some conventional actuators drawn to show their available stress and strain. Note that the active materials, which are above the dividing line, generally produce high stress with limited strain. The conventional actuators, which are below the dividing line, produce high strains at lower

available stress. From this figure, the current interest in shape memory alloys (SMA) is clear. An SMA provides high actuation stress with strains close to those provided by conventional actuators.

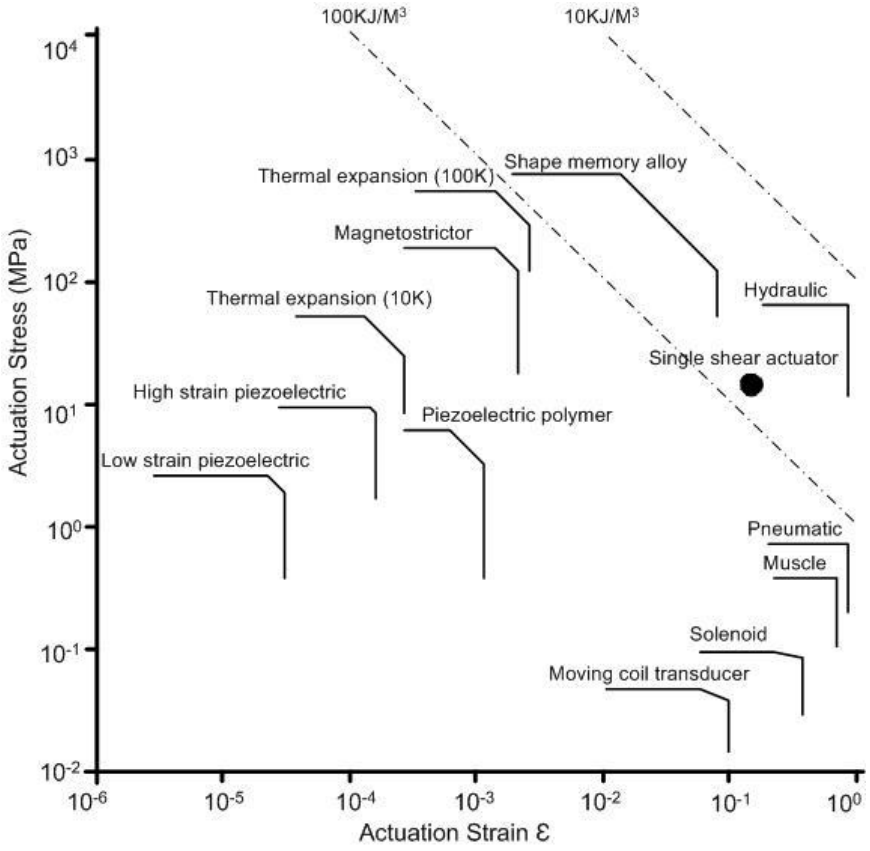

Figure 5. This actuator performance chart (Redrawn from [11]) shows actuation stress – actuation strain relationship.

Nastic materials are under development presently; the goal is to combine hydraulic system's high strain with SMA's high actuator stress. There is no simple way to place nastic materials onto Figure 5. Nastic materials are in a general class. Several

methods can energize nastic materials. Nastic materials can produce strain over a large range. The next two sections present nastic materials in nature and industry.

2.4 Nastic Materials in Nature

In nature, plant movements triggered by environmental changes are nastic movements. However, these movements show non-directional responses to stimuli like temperature, humidity, and sunlight [12]. According to Giurgiutiu [13], If stimulus intensity increases, then the nastic response rate also increases, and usually the plant's internal water pressure induces the nastic movement and produces large strain. Figure 6 shows how nastic movements are classified. Nastic movement is elastic and recoverable changes in plant movement [8].

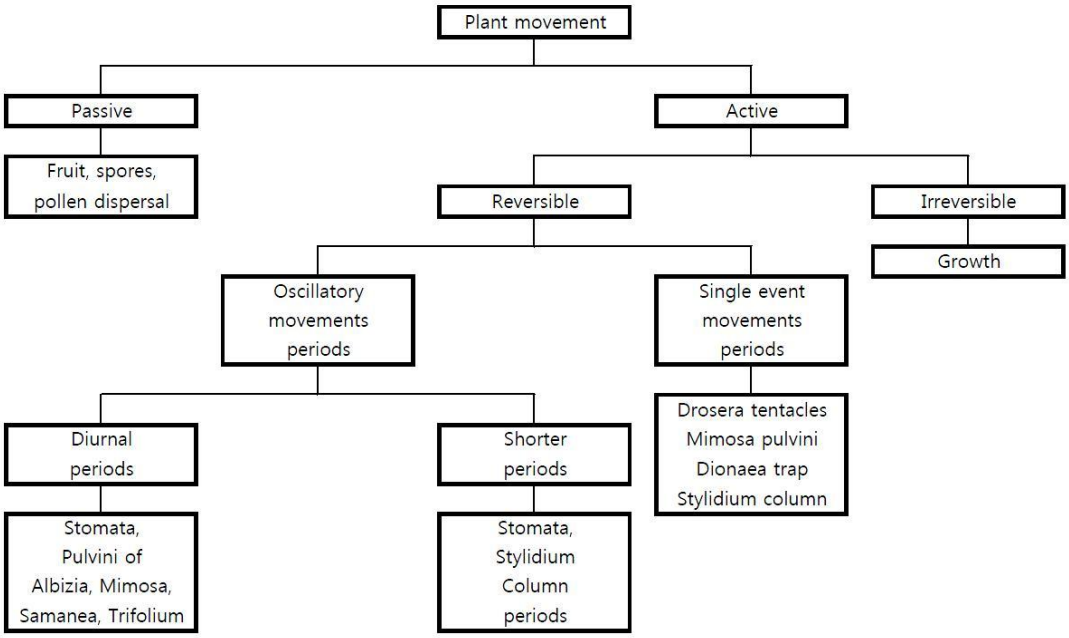

Figure 6. The nastic movements in plants are active, elastic, and reversible (Redrawn from [14]).

Taya [15] analyzed the Venus Flytrap's movement. Figure 7 shows how the trap closes on its prey. Outer cells pressurized by calcium ions and water from inner cells expand and make the 'leaves' leap to the closed position. This movement produces large strains in 0.1 seconds [16].

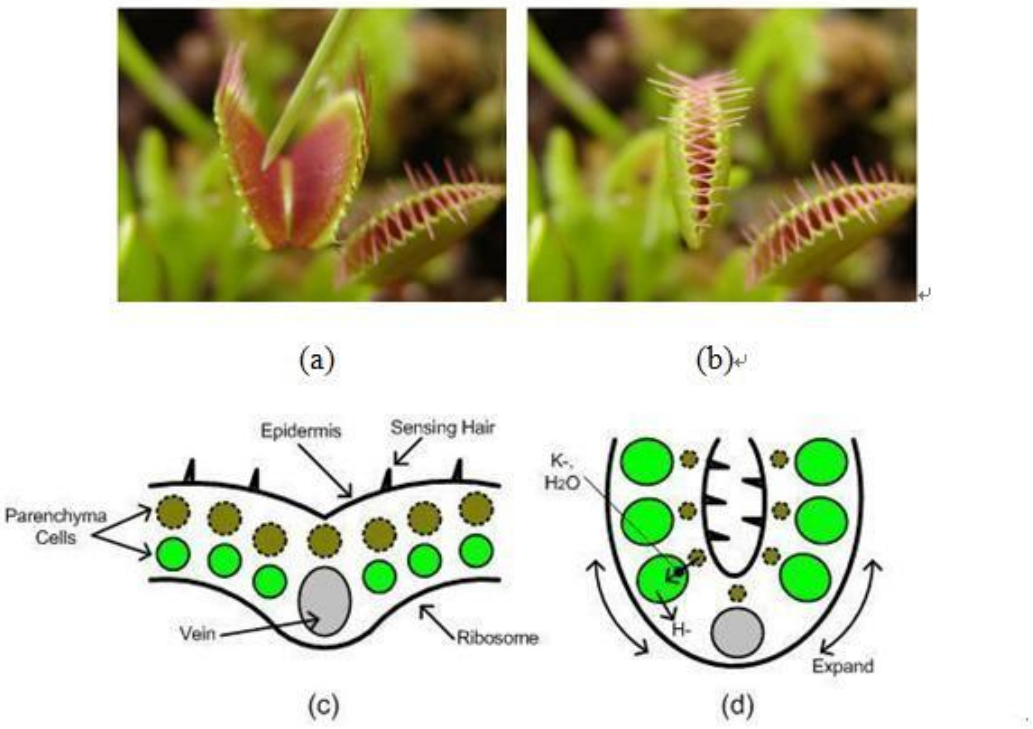

Figure 7. Taya's Venus flytrap. When an insect contacts the sensing hairs, the trap shuts quickly(a, b) [17]. The outer leaf skin's rapid expansion causes closure that involves ion transportation(c, d) (Redrawn from [15]).

Synthetic nastic materials mimic plants that produce large strain in a short time. The active, reversible, oscillatory, and shorter period movement can be good for aerospace applications.

2.5 Previous Nastic Concepts in Industry

Cadogan et al. [3] suggested nastic structures for an inflatable wing. Figure 8 (a) shows that air pressure inflates the tubes. Inflated tubes shorten and produce forces that

perform work on a structure. He applied this to airfoil control. The upper and lower wing skins are deflated tube arrays. As shown in Figure 8 (b), when the lower skin tubes inflate, the skin contracts, and the contractions control the wing.

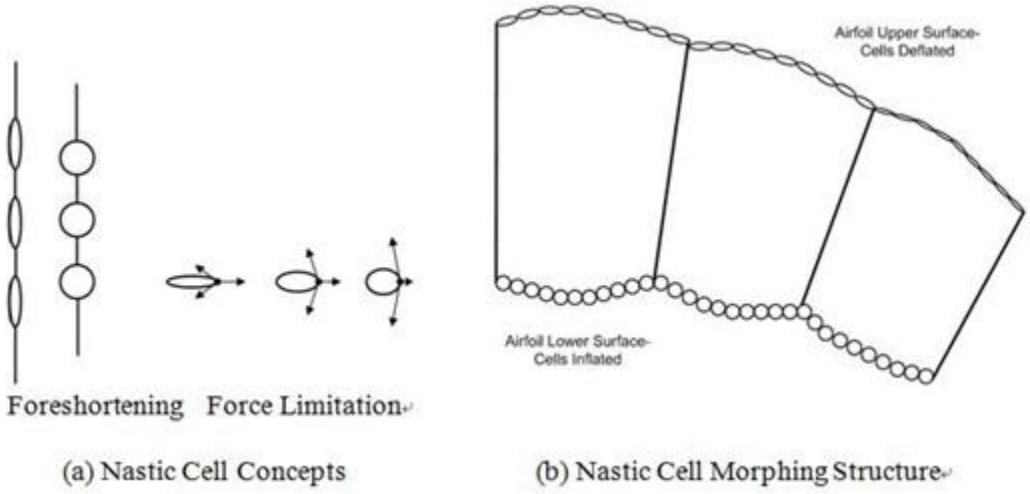

Figure 8. Cadogan et al.'s (Redrawn from [3]) (a) nastic cell shrinks a membrane by inflating repeated cells (b) shows nastic actuated inflatable wing profile.

This concept eliminates cumbersome hinges and joints. Plus, the wings can fold and sit inside the vehicle while stored [18]. This makes it easier to carry the vehicle.

Figure 9 shows another synthetic nastic material. Lee [8] studied a lens shape tube, which is similar to Cadogan's nastic cell, as a shear actuator. The lens-shaped tube is a Kevlar fabric membrane that sits within an elastomer matrix. The membrane holds a bladder that accepts a pressurized fluid. That pressure drives lens shape toward a circle shape and this deformation acts upon the elastomer. Shear deformations to 16% strain were possible.

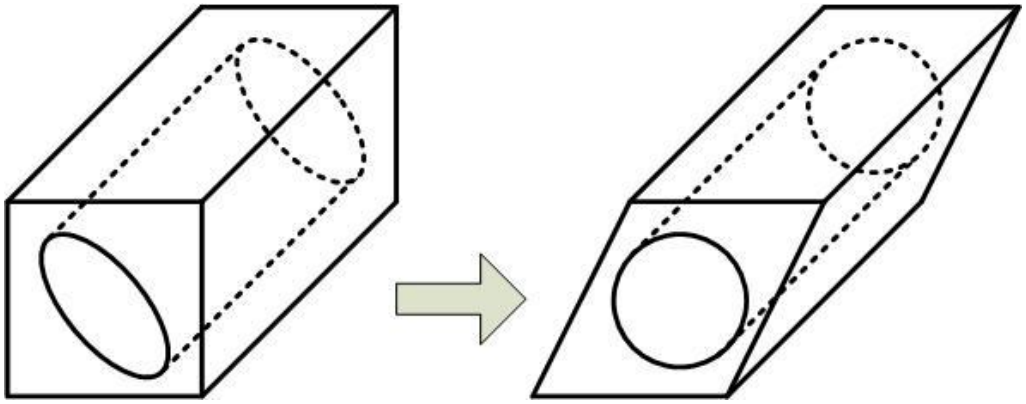

Figure 9. The concept for a nastic cell shear actuator relies on matched expansion and contraction in the elastomer matrix as pressure forces the elliptical membrane to become round. The lens element is 45° to the shear direction before pressure enters the membrane (Redrawn from [8]).

A multiple-element tube array provides larger shear force, but the shear displacement does not increase. The single-actuator's work density is 228.9 KJ/m3 (0.229 MJ/m3), slightly less than SMA, but is much higher than piezoelectric and magnetostrictor materials [8].

2.6 Twisting Beam Using a Shearing Spar

Hawkins at el. [5] suggested that a split-spar could allow a wing to produce controlled twist along a wing at lower power than needed for a closed-spar wing. The split spar is located in the wing profile's center. Figure 10 shows a box-shaped beam profile with a split square spar in the center. A split runs along the longitudinal axis on one side, and this split makes the cross section open. The open section has less torsional rigidity.

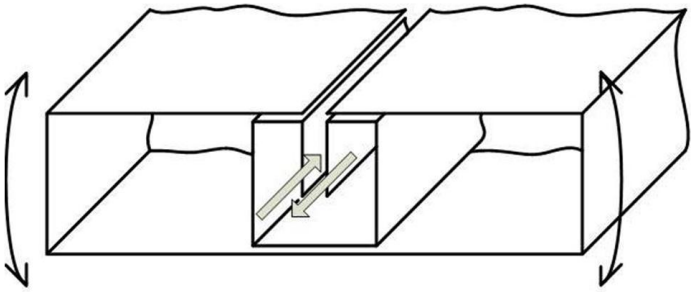

Figure 10. The square spar is the main stiff structure and it runs though the wing's outer skin, which a rectangular shell represents here. Generating two equal and opposite shear stresses between the split gap-flanges makes the wing twist.

With the section open, the spar can twist with less force. An active material actuator placed between spar's flanges can twist the spar if it generates shear displacement that shifts the flanges in opposite directions. The drawback is that an open cross section spar is not appropriate for a main wing because the open spar has low torsional rigidity. Lee [8] proposed actuating a split spar by nastic materials.

2.7 Locking Methods

One challenge for morphing wings is to keep them stiff. The wings must be stiff when wing shape should not change, for example, during cruising, and stiff wings avoid catastrophic flutter events that could destroy the wing. However, the high stiffness would be a big obstacle when the shape needs to transform for landing or takeoff. Mechanical clamps can lock the spar. However, conventional mechanical clamps shown

in Figure 11 are mechanical joints, which are the conventional wing's drawback. Another way to lock the spar is to maintain applied forces that transform the wing shape. While the forces act, the wings keep their stiffness. This method wastes energy while maintaining a shape.

Figure 11. Top row: Pipe clamp / 2nd row from top: F-clamp or bar clamp, one-handed bar clamp, wooden hand screw / 3rd row: spring clamp, C-clamp, cam clamp [19].

In this study, a high stiffness, thermoplastic polymer is the locking material. The material fills the gap, bonds to both flanges, and closes the cross section. The closed cross section spar is hard to twist–it regains its high torsional rigidity. When the spar needs to transform, applying heat to soften the polymer makes the spar an open cross section that is relatively easy to twist. Solidified locking polymer can lock the spar

elastically and let the system keep a shape without using energy. The locking polymer must have high elastic modulus, small stress relaxation, and a reasonable glass transition temperature. The melting temperature must be higher than the use temperature, yet not so high that melting damages the wing or requires too much energy. Polymers have higher stress relaxation and lower elastic modulus than metallic materials; therefore, the system requires careful design and material selection.

2.8 Ultem's Characteristics

In this work, 0.5mm thick Ultem film provides a high elastic modulus model locking material. Ultem is an amorphous thermoplastic polyetherimide (PEI) products manufactured by Saudi Basic Industries Corporation (SABIC). It shows exceptional thermal resistance, high strength and stiffness, and broad chemical resistance [20].

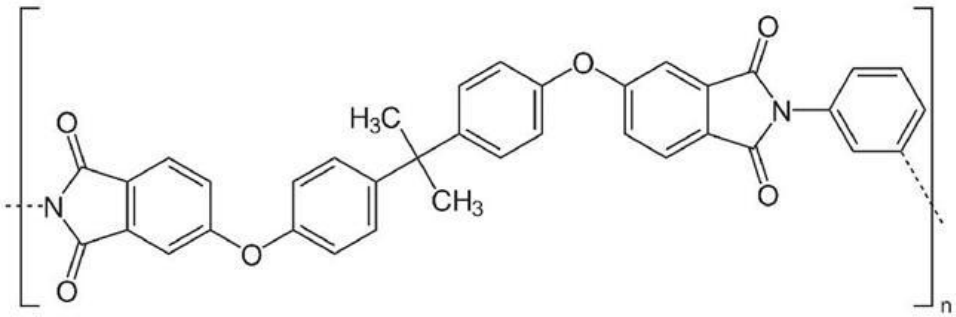

Figure 12. Ultem's molecular structure contains many aromatic rings on the main polymer chain [21].

Figure 12 shows Ultem's molecular structure. The aromatic rings in its structure increase mechanical performance. According to Port Plastics, Ultem 1000 has a 3.28GPa elastic modulus and a 215^{o}C of glass transition temperature [22]. Ultem 1000 melts at 349 ^{o}C according to Parker TexLoc [23]. These properties produce phenomenal strength at elevated temperatures, low creep sensitivity, and uniform coefficient of thermal expansion that can be suitable for this project.

The Ultem 1000 series has relatively simple processing procedures because it does not need glass reinforced. The processing methods are injection molding, extrusion, and extrusion blow molding. This polymer however is notch sensitive, so the design of injection and extrusion die requires a generous radius on external and internal corners.

The Ultem has a drawback: it degrades when heated, even when heated in a vacuum [24]. Although Ultem cannot provide a locking effect that works for 10s to 1000s of cycles, Ultem does demonstrate what is possible if there is a material with better thermal cycling characteristics.

3. METHODS

3.1 Finite Element Analysis

The spar model runs in ABAQUS. This procedure helps a designer choose dimensions and find performance for the spar. A prototype spar was built based on this analysis. Finally, FEA analysis verified the prototype results.

3.1.1 Spar Design and Twisting Angle Defined

The design target is fixed-wing aircraft spar that is strong and stiff. Alloy 6061 aluminum is a common alloy for general use; it has good manufacturability and weldability. The Al6061-T6 elastic properties are :

- Young's modulus : 68.9GPa
- Poisson ratio : 0.33
- Yield strength : 276MPa

according to ASM material information [25].

One mm thick plate provides good torsional rigidity with small radius bends. Plates thinner than 1 mm reduce the torsional resistance, and thicker plates make the bend radii too large. Figure 13 shows the spar’s dimensions. It is 5m long for application in a fixed-wing aircraft. The cross section size is 40cm × 40cm, and the split gap on one rectangular face is 0.5mm. On each side of the gap, 30mm long flanges extend into the

spar's interior. The active material and locking material go between the flanges to drive and lock the twisting.

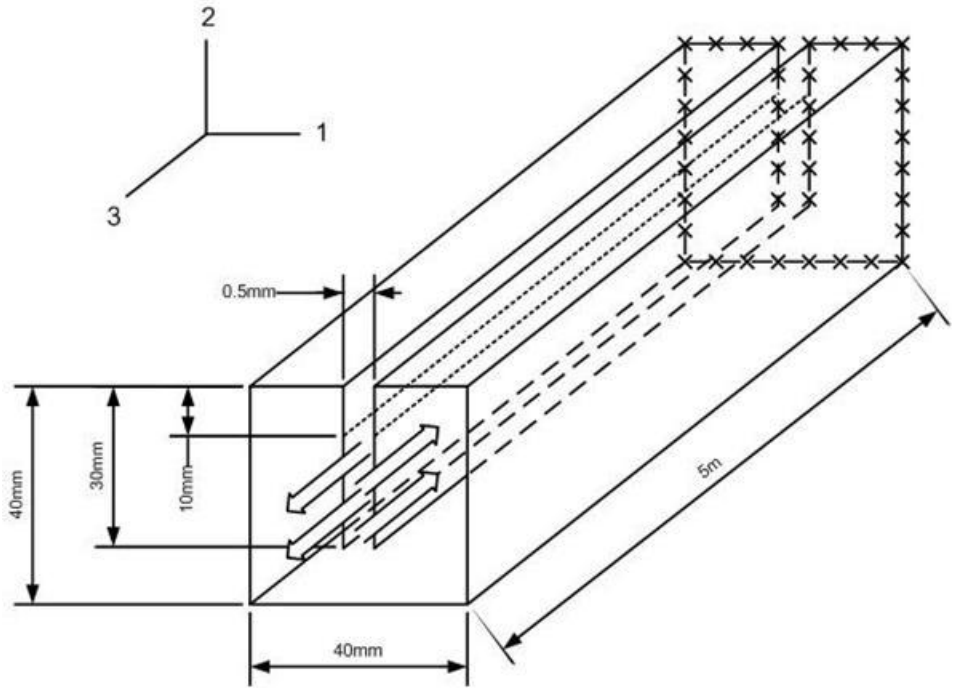

Figure 13. This spar's dimensions are not from any particular wing; it is a generic spar.

The square spar might not twist simply like a circular spar. The square's twist angle might be eccentric. Figure 14 shows how this thesis defines twist. The twist angle is the angle between a vertical line and the line drawn from node 1 to node 2 when the model twists, as Figure 14 shows.

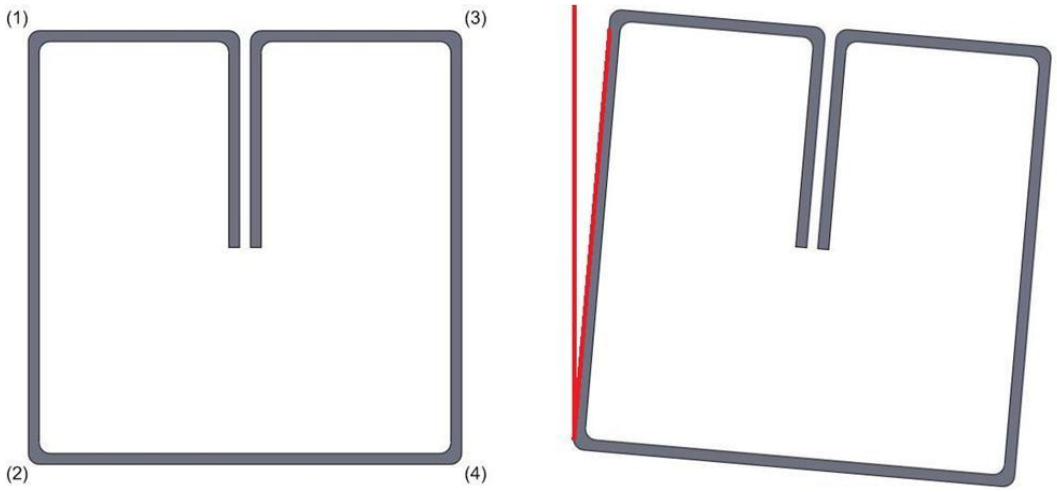

Figure 14. Twist is the angle between a vertical line in the global coordinate system and the line drawn from node 1 to node 2 (or node 3 and 4) when the model is twisted.

This spar design does not apply to any specific wing. First, it has a uniform cross section for its 5 m length; an actual spar cross section would have a variable cross section along the length. This simple design allows for testing the locking concept.

3.1.2 Load and Boundary Conditions

The load and boundary conditions affect the spar's twisting angle and torsional spring constant. Figure 15 shows the conditions. All edges at the distal end are fixed. i.e., clamped. This provides a torsionally stiff condition that matches a wing mounted to a fuselage. The proximal end is free; this freedom allows the spar to twist.

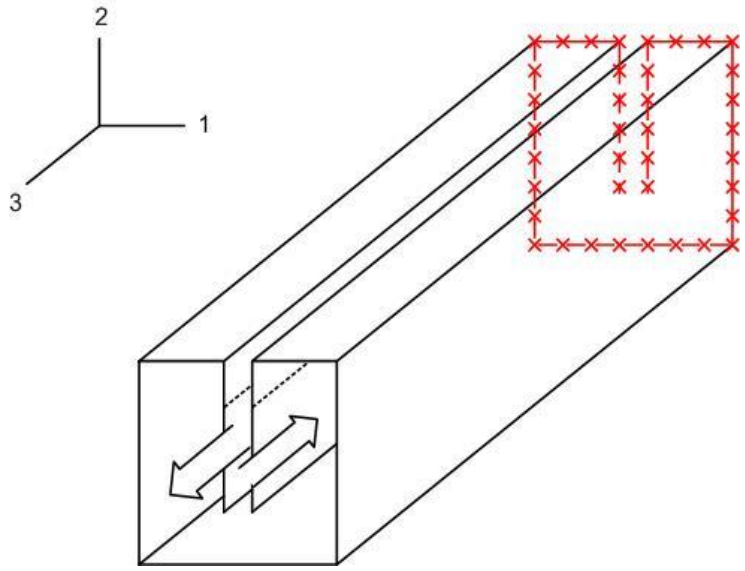

Figure 15. The spar has a fixed boundary condition at one end while the other end is free.

3.1.3 Meshing

This model has extremes in dimensions that make it difficult to model with 3D solid elements. The 1 mm wall and 5 m length requires too many elements. Therefore, shell elements formed the mesh and accommodated both dimensions. The analysis used simple linear elements rather than quadratic elements for reasons discussed in the results.

3.1.4 Material Selection for the Locking Material

Locking material should have large stiffness at the spar's operating temperature so the material can lock in the twist without help from the actuators. The locking material should be reusable; a thermoplastic material might be capable. Heat softens the

locking material, and cooling solidifies it. Ultem, polyetherimide (PEI), can satisfy these conditions. SABIC Innovative Plastics manufacture Ultem in their PEI product family. It could be little difficult to soften because it has a high melting point, but it has high elastic modulus, tensile strength, and stiffness.

The locking material sits above the region where stress is applied. Figure 16 demonstrates volume, in red, that contains the locking material. The locking material is 0.5mm wide, 10mm high and 5m long. The material sits over the nastic material and does not disturb actuation.

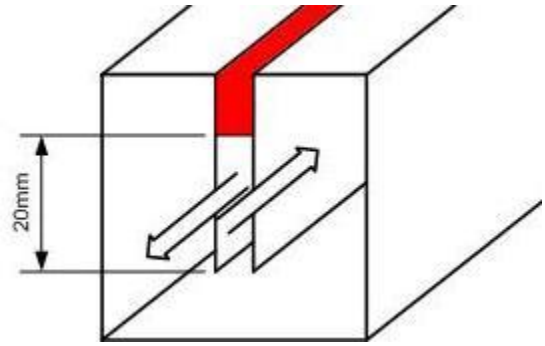

Figure 16. The locking material sits in the red volume. Shear forces from the nastic material act on the bottom of the flanges over 20mm vertically.

3.1.5 Locking Ratio

Ideally, the nastic material must produce the twist and the locking material must maintain that twist. The locking material and the spar are elastic components, and the locking material becomes stiff after it solidifies. Therefore, the spar must spring-back somewhat to load the locking material through shear. The spar and locking material are

opposed springs that reach equilibrium. This means that it might be necessary to over-twist the spar before locking it. The result section presents the locking ratio calculation between the spar and the locking material analytically and experimentally.

3.2 Experiment

This section describes the tensile test, the stress relaxation test, and the lap shear test for obtaining the Ultem film's performance. It explains fabrication, calibration, and locking demonstration methods for a prototype spar section.

3.2.1 Locking Material Mechanical Properties

The Ultem film chosen as a locking material is a general use material; therefore, the vendor sold it without certified properties: elastic modulus, stress relaxation, and adhesion to aluminum.

3.2.1.1 Tensile Test

Thin polymer sheet tensile tests should follow standard ASTM-D882. Figure 17 shows the specimen is 300 mm long, 25 mm wide and 0.5 mm thick. Figure 17(b) shows

the specimen with masking tape placed to cushion the gripping areas. Without this protection, the test machine grip might damage the specimen, which breaks at the grip.

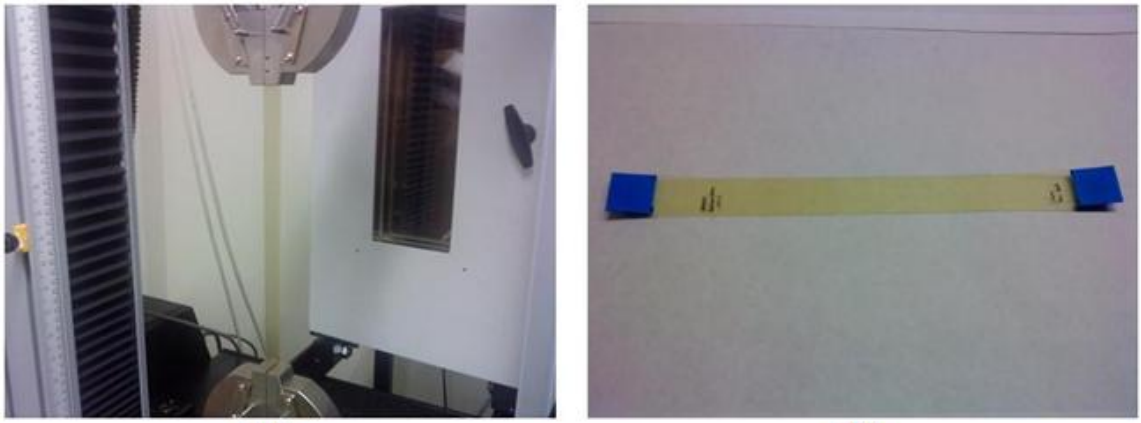

Figure 17. (a) Tensile test for 0.5mm thickness Ultem film (b) The blue masking tape helps prevent breaking at the grips.

The tape could cause slipping during the experiment; therefore, the grips were tightened securely and slip indicators were drawn on the specimens at both grips. If the specimen slips, the distance between the line and the grip increases and the experiment is cancelled.

3.2.1.2 Stress Relaxation Test

The stress relaxation test shows how load falls while polymer rests at a fixed extended length. Figure 18 shows the 100 mm long, 12.5 mm wide, and 0.5 mm thick specimens specified by test method ASTM E328.

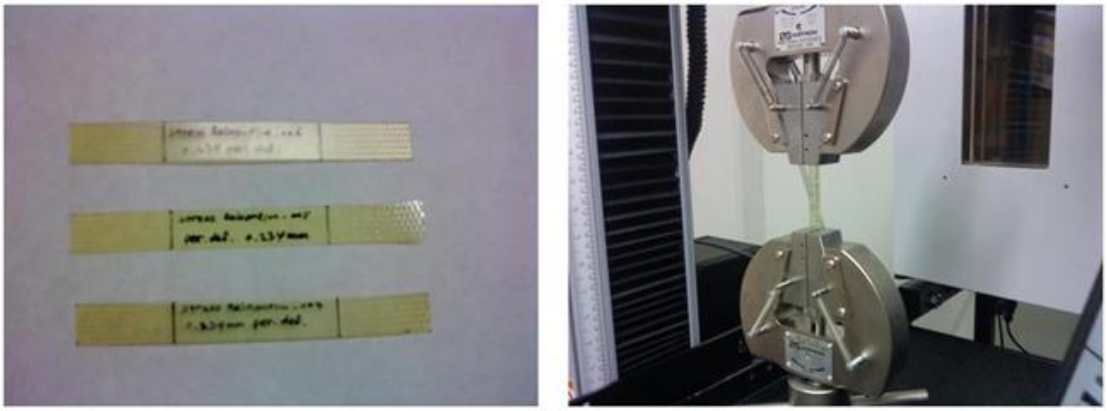

Figure 18. (a) The stress relaxation specimen is smaller than tensile stress specimen. (b) Stress relaxation test specimens have no protection on gripped areas because any slip between masking tape and grips affects the relaxation.

The specimen does not need tape to protect its gripped areas. The cross head extends and holds the specimen at 2% strain so the load is much lower than the tensile test. The masking tape might slip and affect the relaxation response.

3.2.1.3 Lap Shear Test

The single lap-shear test measures the Ultem film's bonding ability. Figure 19 shows the test procedure. First, Ultem film was placed in-between aluminum panels as shown in (a), and this sandwich was clamped and baked Figure 19 (b) and (c) show. The clamping applied pressure, and helped bond a little. After removing scraps, the panel went into the tensile test machine as shown in Figure 19(d).

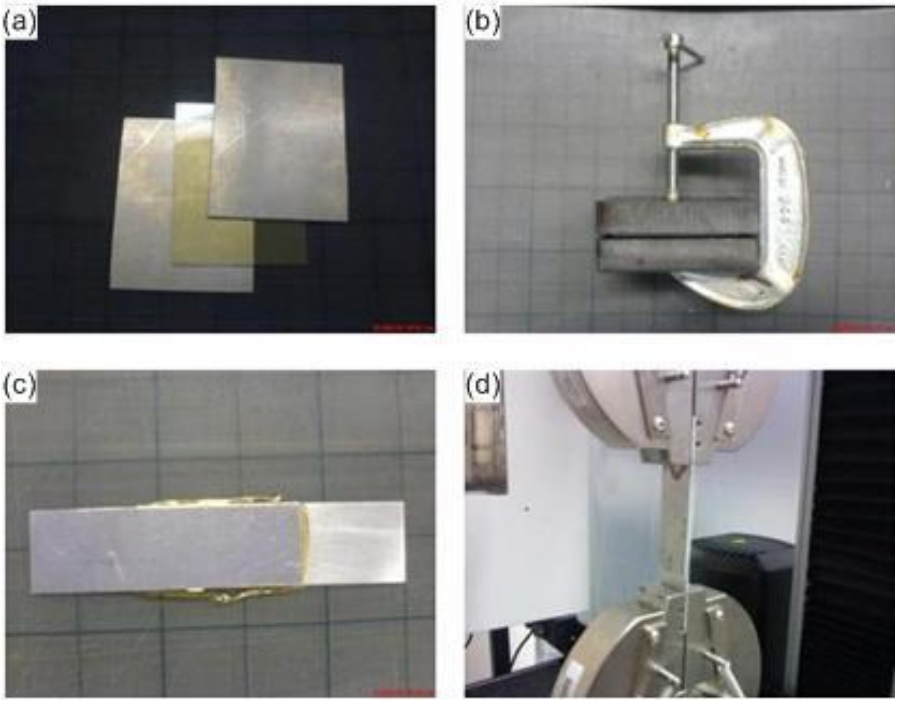

Figure 19. (a) Place Al plate-polymer sheet-Al plate order. (b) Clamp the sandwich panel. (c) Bake the panel for 20min in 500^{o}F. (d) With the scrap filed off, the panel went to the tensile test machine.

The aluminum plates were 23.54 x 1 x 83.40 mm and the bonded region is 52.58 mm long. Applying heat for 20min while clamped in a 500^{o}F in the oven softened the Ultem film and stuck with aluminum panels.

3.2.2 Prototype Spar Section

It was beyond this project's resources to build and test a 5 m aluminum spar. Therefore, a short spar represented the 5 m spar's free end.

3.2.2.1 Short Spar Fabrication

The short spar‘s dimensions are close to the ideal one analyzed in FEA, except that the overall length is much shorter and the flange size is 20mm long. Figure 20 presents the 30 cm long prototype spar's dimensions.

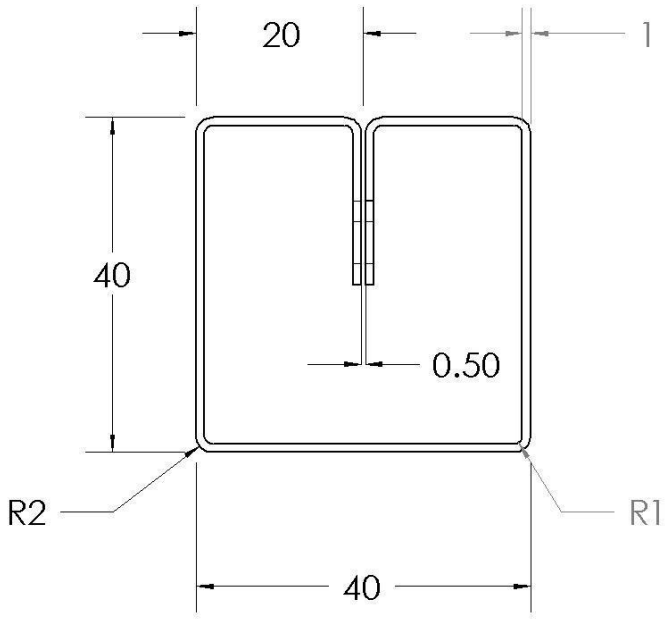

Figure 20. Spar cross section dimensions are similar to the 5 m spar’s dimensions. The model spar is only 30 cm long.

As shown in the magnified front view, Figure 20 bending flat aluminum plate into the right cross section introduced a radius at the edges. In other words, the cross section will not be a perfect square when bending forms the beam. This bend radius affects the top of the flange, and reduces the region where the Ultem contacts the flange.

The flange surfaces were cleaned and sanded at 45 degrees with 150 grit sandpapers. This surface process helped the thermoplastic polymer stick on the aluminum when heating softened the polymer. In a real application, the fabrication method and surface treatment would be design parameters. This experiment followed the analysis; the best possible beam was made and tested—the beam did not match the ideal design.

3.2.2.2 Spar Spring Constant

The model spar's spring constant was measured in a tensile test frame. Figure 21 present the procedure. Bolts and nuts clamped tabs, which extend the flanges beyond the model spar's length, to the flanges as shown in Figure 21(a).

Figure 21. (a) Tabs connect to the spar section's flanges with bolts and nuts. (b) Tensile test machine fixed with the tabs show relation between force applied and displacement.

Figure 21 (b) shows that the tabs make it easy to place the spar on the tensile test machine. The spring constant was found manually. After mounting the spar and zeroing

the load cell, the crosshead was moved in small increments to 2 mm displacement. The load/displacement data, when fit with a least-squares line, provided the beam's spring constant, which is the slope from the least squares fit.

3.2.2.3 Locking Demonstration

For the locking demonstration, a support holds the spar in twisted state. It is 1-inch thick aluminum 6061-T6, the same material with the spar. Tabs connected on each flange end link this support and the spar. Figure 22 presents the assembled prototype spar and its support.

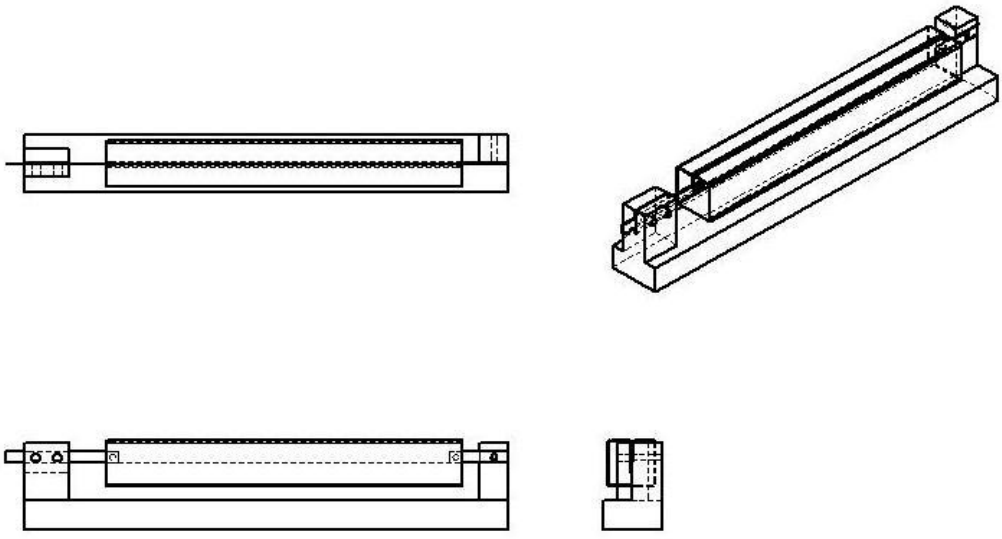

Figure 22. The spar section with its support.

The support grips the spar tabs. One end of the support fixes the spar tab with a bolt; this end is marked with a red circle in Figure 23. The other end tab can slide in

longitudinal direction shown as the red arrow. When the sliding tab reaches a specific displacement, a clamp holds the tab in place. The twist depends on the sliding tab's displacement. This appliance makes it easy to get various twists.

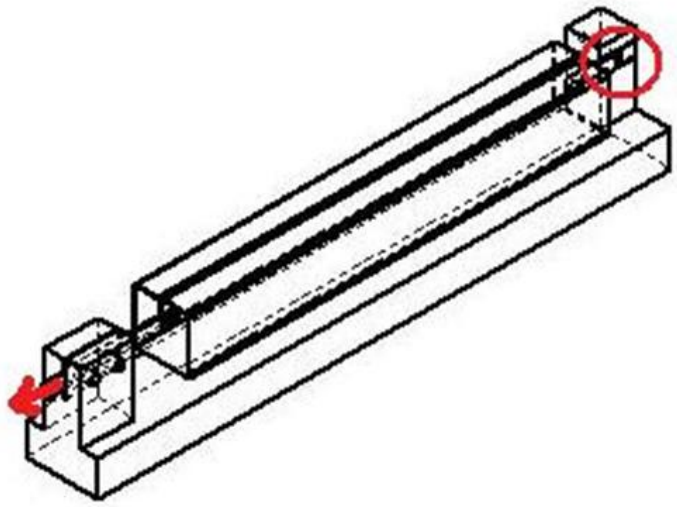

Figure 23. Figure shows a way that makes the spar twist without installing the nastic material. One tab is fixed (circled), and force displaces the other end (arrow).

To soften the thermoplastic locking material, the spar and support went into an oven. This experiment has one big challenge. The twisted spar has internal strain field caused by applied forces for twisting. The heat energy for softening the locking material may affect the twisted spar, and relieve the internal strain in the spar. In other words, the spar can twist and spring back at room temperature, but the hot oven could anneal the beam and remove spring back. The annealing provides permanent deformation. The temperature and time that soften the locking material without annealing the spar was found. As shown in Figure 24, the twisted spar without locking material and the lap-

shear test panel simultaneously went into the oven. If too high and held for too long, the oven temperature would soften the Ultem film but it might anneal the spar. On contrary, the spar would keep elasticity but the Ultem film between the panels might not soften at too low temperature and short time. The optimum temperature and duration satisfy softening the film between panels but not annealing the spar.

Figure 24. In this test, the twisted spar and the lap shear test panel where simultaneously heated in an oven to find a temperature that softened the locking material without annealing the spar. The locking polymer had to form a good bond with the aluminum plates.

After finding out the particular duration and temperature for softening the locking material but not annealing the spar, the twisted spar with the Ultem film between the spar flanges went into the oven. After solidifying the Ultem film, the spar should stay twisted without the support, and the spar should be trying to spring back.

4. RESULTS AND DISCUSSIONS

4.1 Experimental Results

This section presents the locking material's mechanical properties, spring constant, and the prototype spar locking demonstration experiment.

4.1.1 Locking Material Mechanical Properties

This section reports the tensile test, the stress relaxation test, and the lap shear test results for the Ultem film's performance.

4.1.1.1 Effective Elastic Modulus

Polymer generally presents non-linear elastic deformation as shown in Figure 25. This non-linearity makes it hard to obtain constant elastic modulus. At 2% strain, the plot shows nearly linear deformation with a 2.75GPa elastic modulus; an experiment must verify this prediction.

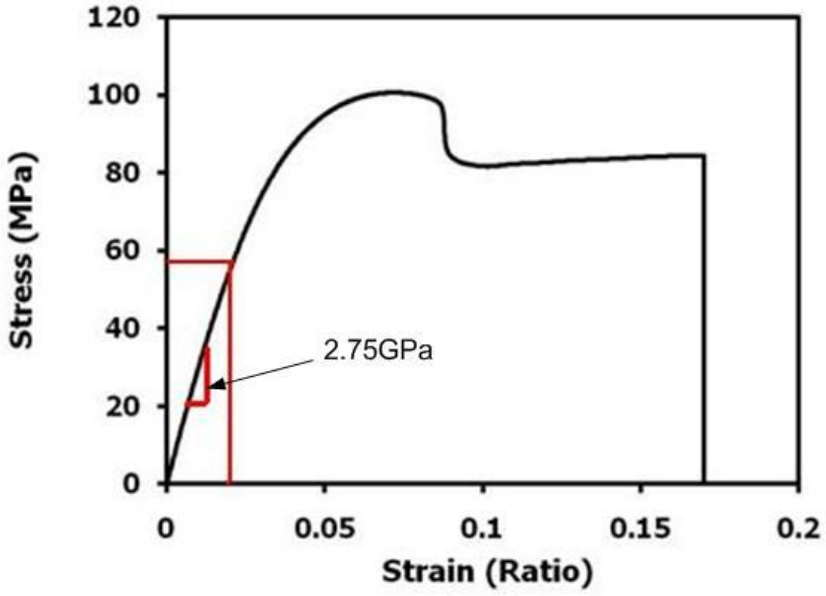

Figure 25. Linear region is hard to define in this test result.

To verify that 2% strain causes only elastic deformation, 2% strain was applied and released immediately. Figure 26 shows the tensile test specimen with a circle drawn on the specimen's surface. A circle drawn on the specimen surface before the experiment did not show permanent dimensional change after the test. Figure 27 shows the circle before and after the experiment.

Figure 26. To verify that 2% strain causes only elastic deformation, 2% strain applied with a tensile test machine was released immediately.

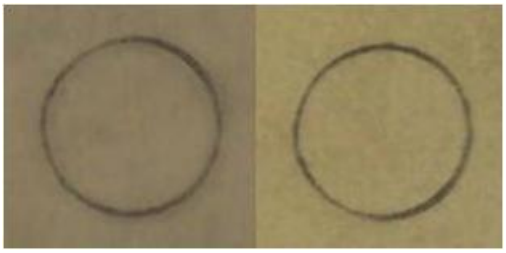

Figure 27. A circle drawn on the specimen surface did not change its shape during the test; therefore, the deformation was elastic.

The mean elastic modulus, 2.31GPa ± 95.44MPa, comes from three repetitions. Figure 28 presents the immediate tension-and-release data for effective elastic deformation. The mean value slope, 2.31 ± 0.10 GPa, is almost linear.

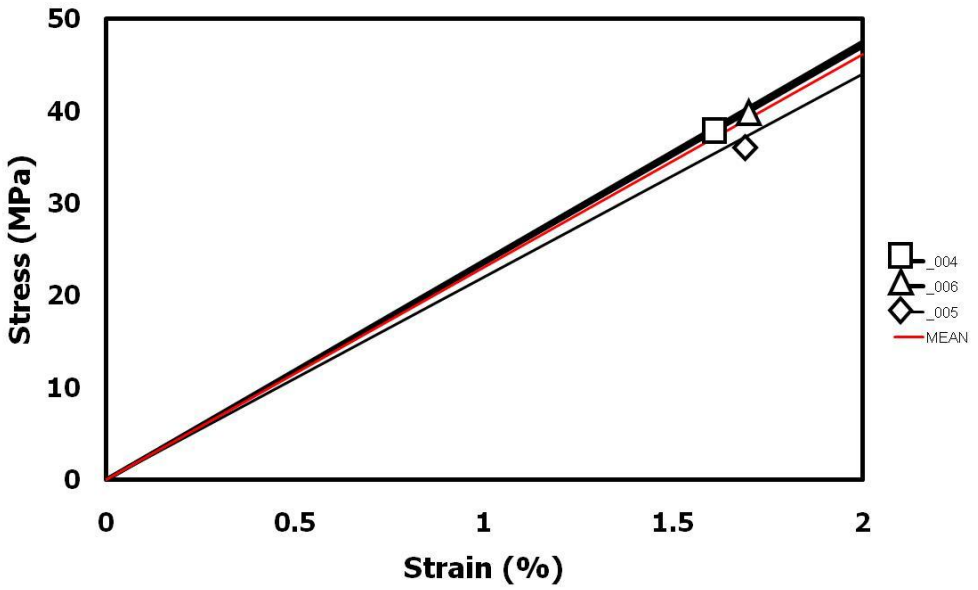

Figure 28. Strain up to 2% presents linear appearance.

4.1.1.2 Stress Relaxation Test

This project targets an application for the fixed wing aircrafts. The operation hours should be long enough for flight hours. If the locking material relaxes during flight, the wing loses its stiffness. Three stress relaxation tests with Ultem film appear in Figure 29. Just after stopping the crosshead, the load drops quickly, and is getting slow the reduction rate. Eventually, the load dropped almost 20% in 10 hours. This relaxation affects the Ultem's elastic modulus. Equation (1) shows the simple stress-strain relation. From the equation (1), one obtains the equation (2) that presents a connection between the elastic modulus and load.

$$\sigma = E\varepsilon \qquad \frac{F}{A} = \sigma \qquad \textbf{(1)}$$

$$F = E\varepsilon \times A \quad \textbf{(2)}$$

While the load drops, the strain, ε, is constant during the stress relaxation test. The Area, A, should be the same or reduced in a negligible quantity. Consequently, the elastic modulus, E, will decrease with the same fraction, i.e., 20%, of the load drop. The section, 4.2.4 Analytic Locking Ratio, will cover how much relaxed elastic modulus affects the locking ratio.

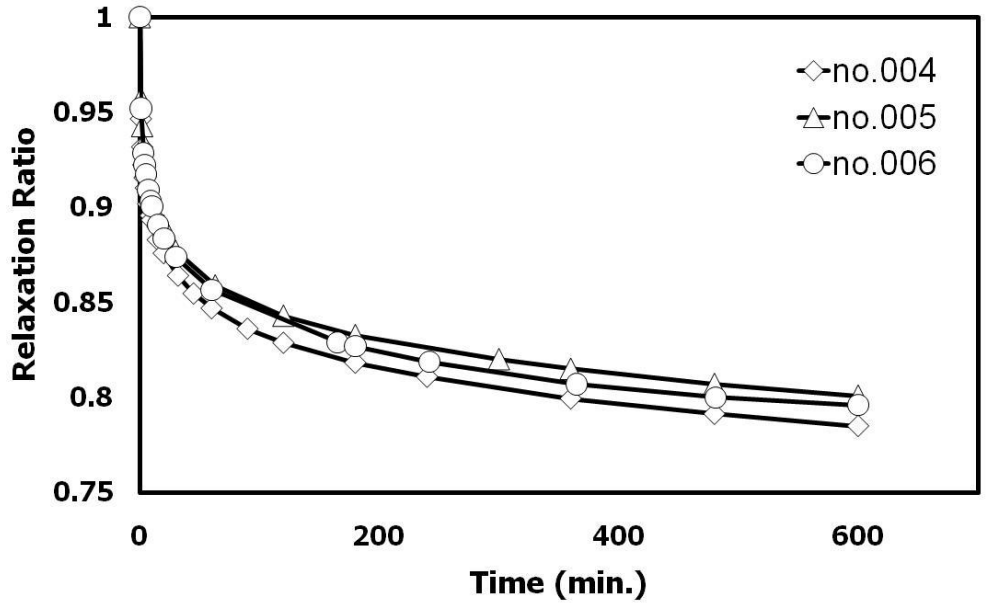

Figure 29. The force dropped 20% in 10 hours.

4.1.1.3 Lap Shear Test

The lap shear test finds the locking material's bonding ability and shear stiffness. Figure 30 presents test specimens from two trials. Specimens 001 and 002 exhibit

adhesive bonding and interfacial fracture. The specimen 002, (b), presents more jumping facture than 001 does, (a), according to Figure 31. The Ultem has high toughness, so it would not show a cohesive bonding.

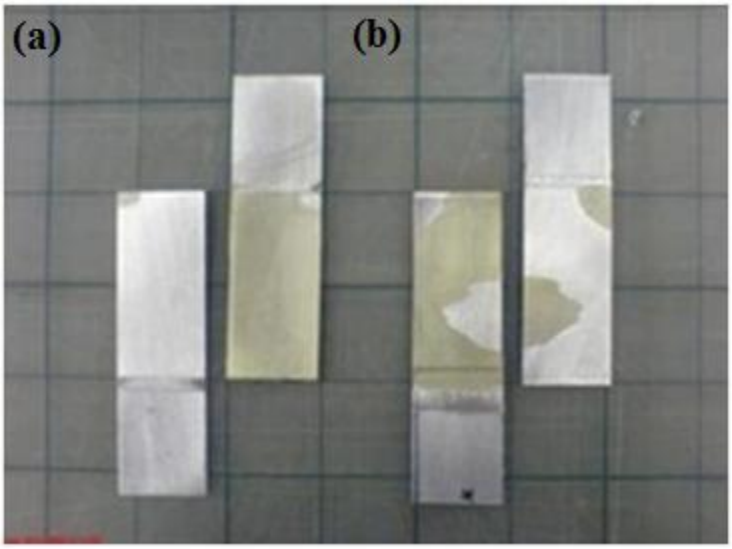

Figure 30. Single lap shear test specimen (a) no.001 (b) no.002. Specimen 002 shows more fracture jumping from one interface to the other compared with 001.

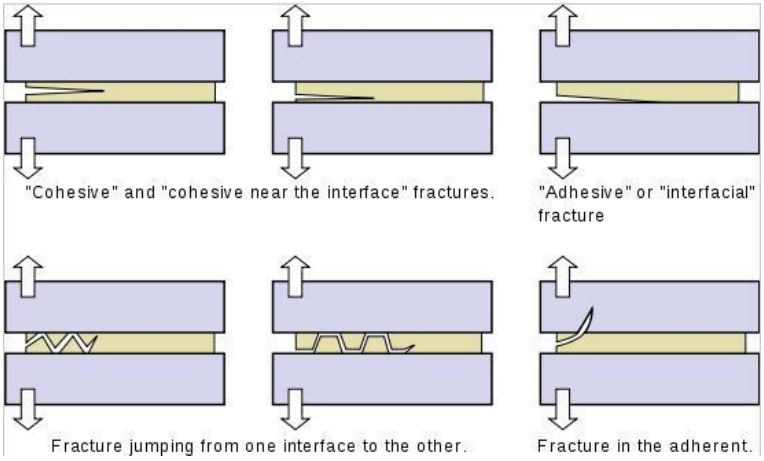

Figure 31. This diagram shows typical adhesive joint failure mechanisms. [26].

Depending on the bonding conditions, the two specimens present various toughness and stiffness as displayed in Figure 32. The specimen 001 slope shows 286.45 MPa stiffness when there is adhesive bonding and interfacial fracture. Otherwise, the specimen 002 shows 277.82MPa. The area under the curve for 002 is much larger than 001; the 002 specimen has higher toughness.

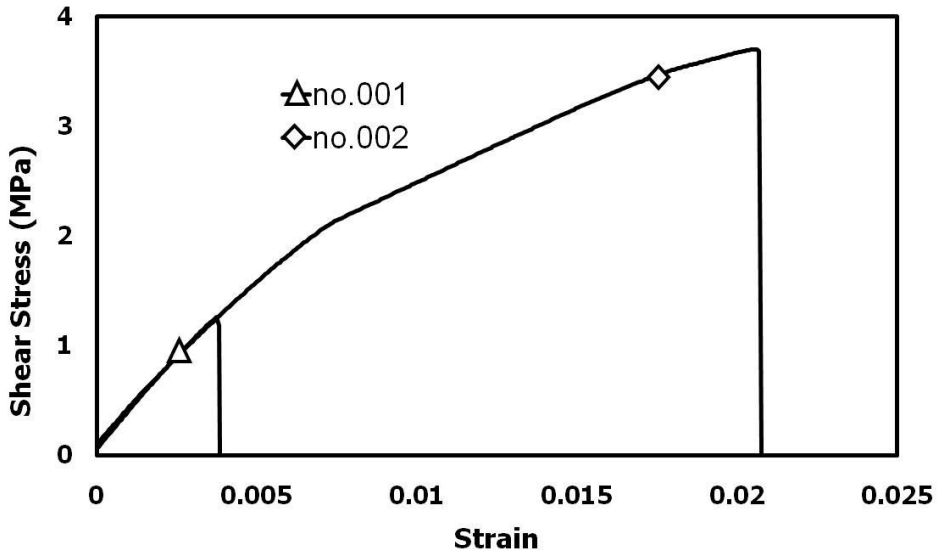

Figure 32. Specimen 001 and 002 stiffness is 286.45MPa and 277.82MPa respectively. The toughness varies with the bond quality.

4.1.2 Spar Spring Constant

Assume the prototype spar section is a big spring. Applying tensions on each tab simply makes the spring extend. The tensile test system provides the data for Figure 33. The results show perfect linear, and the slop, spring constant, is 39.72KN/m.

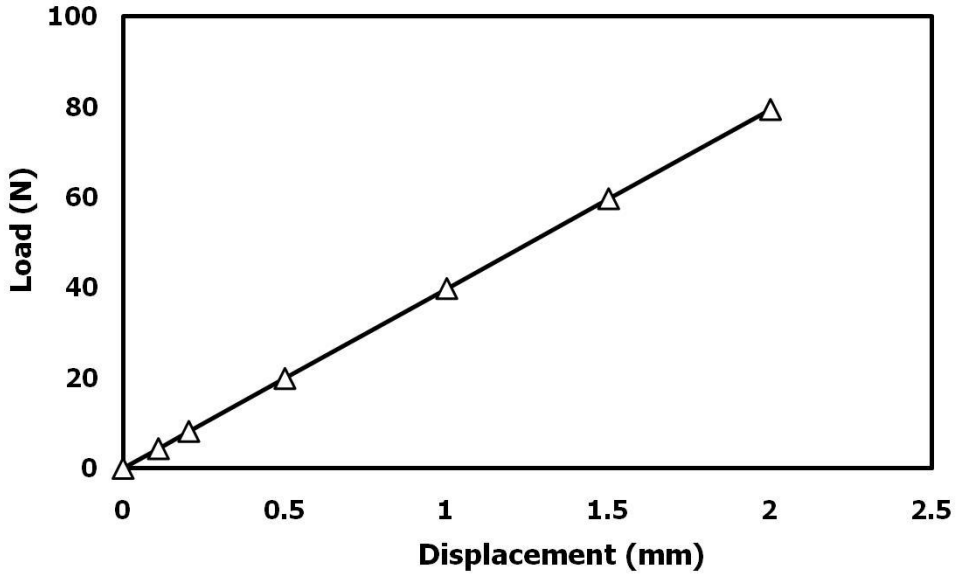

Figure 33. The prototype spar's spring constant is K=39.72KN/m.

Figure 34 the gripped spar in a twisted state. The spar shows about 8^{o} twisting when the free end tab displaces 2mm. After applying the displacement, a bolt holds the twist. This twisting value matches the FEA result.

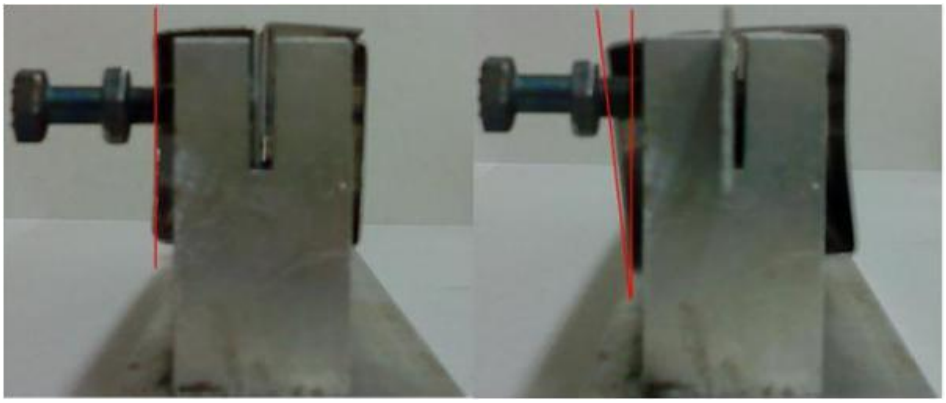

Figure 34. This front view shows that the spar twists 8° when the tab moves 2 mm.

Measuring exact twisting might be impossible because the spar surface is not perfect flat. The best estimation for twisting degree would measure the angle in front view picture by software.

4.1.3 Experimental Locking in Prototype Spar Section

Applying heat under tension affects deformation in aluminum structures. The heat energy relieves the stress in the aluminum and makes the deformation permanent. Thus, low temperature and short duration treatment will minimize the annealing effects. From trial and error, applying 288℃ (550℉) for 15 minutes softens the Ultem film without annealing the spar. Figure 35 shows the twisted spar with its support in the electric oven.

Figure 35. Apply heat 288^{o}C (550^{o}F) to the twisted spar with placing on the locking material during 15min.

Cooling the twisted spar solidifies the softened Ultem film. This hardened Ultem film is able to hold the spar's spring back force. When taken from the support, the spar shows the applied displacement, 2mm, as demonstrated in Figure 36. As the FEA analysis predicted, the spar did not spring back.

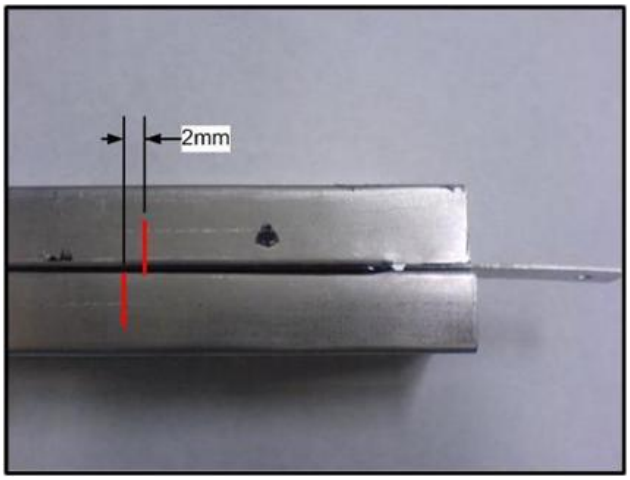

Figure 36. No spring back was observed after solidifying the locking material.

The solidified Ultem locks the spar, and maintains about 8 degrees twist –the FEA results predicted 7.91 degrees twist. Figure 37 demonstrates that the Ultem film holds the twist without spring back.

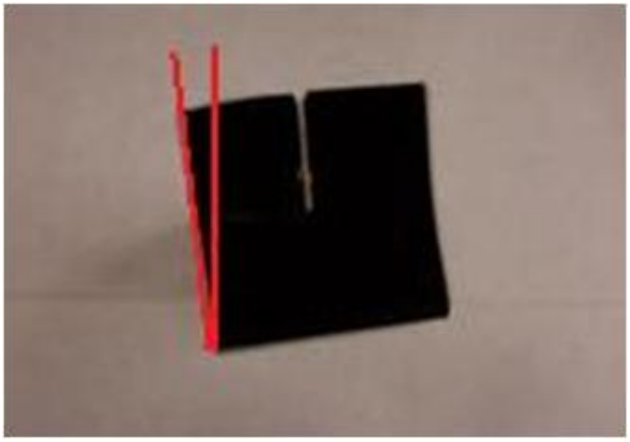

Figure 37. A 2mm displacement in z direction twisted the spar section. About 8^{o} twisting remains after solidifying the softened locking material.

This section verified FEA results and the analytic solution. The FEA results predict that applying 2mm displacement in Z direction twists the spar section about 8 degrees. The analytic solution anticipates that the locking material hold the spar without spring back.

4.2 FEA Results

This section covers numerical analysis results for the 5 m long ideal FEA spar and the prototype spar section. It presents the relation between stress and twist; the prototype and ideal FEA spar locking analysis; and FEA verification for the spar section.

4.2.1 Twist Analyzed Numerically

This section presents three results:

- What mesh sizes are reasonable for the 5m spar model?
- How much shear stress should be applied to twist the spar and where the shear stress must be applied.
- How the twists and shear stresses are related.

4.2.1.1 Meshing

The first issue with the mesh was to select appropriate elements. Quadratic elements have more nodes than linear elements, and they can more accurately model this problem. However, this meshing study found that the quadratic element model results were less than 0.5% different from a linear element result. Therefore, linear quadrilateral elements were used in this analysis.

The shear stresses, $\pm$450Pa, produce 2.11^{o} twist at the free end. Figure 38 shows that the model converged over a large mesh size range. The twist angle shows only 0.01% difference for mesh sizes from 2mm to 12mm. Even the 40 mm mesh is only 0.025% from the 2 mm mesh result. Therefore, any size between 2 mm and 40 mm is appropriate for analysis. This analysis used a 2 mm mesh with linear quadrilateral elements that kept the model small with convergence.

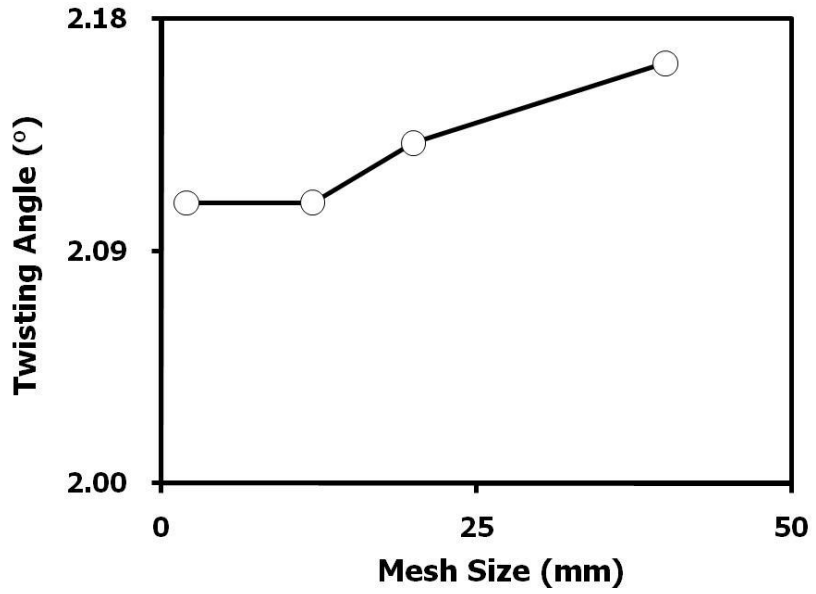

Figure 38. The twisting angles have less than 0.01% difference from 2mm to 12mm mesh size with same load and boundary conditions. This graph shows that the FEA model converged.

The clamped end might need to be analyzed with fine meshes because the spring constant may present jumping at the fixed end boundary condition. Fine meshes take too much computational resource, so a biased mesh was used. Near the clamped end, the mesh size is 0.33mm, and the size is getting larger up to 4mm. The difference in locking ratio between regular mesh and biased mesh will be shown in the 4.2.4 Analytic Locking Ratio section.

4.2.1.2 Shear Stress Application

The active material must produce opposed shear stresses on the flanges, which are 40 mm high and 5 m long. Figure 39 presents the load directions for twist. The shear

stresses should act on the flange surfaces from the flange free edge over 20mm up from the free edge for most or all the spar's 5 m length. If the stresses act on the entire flange surface, the twisting includes the large eccentric displacement shown in Figure 40.

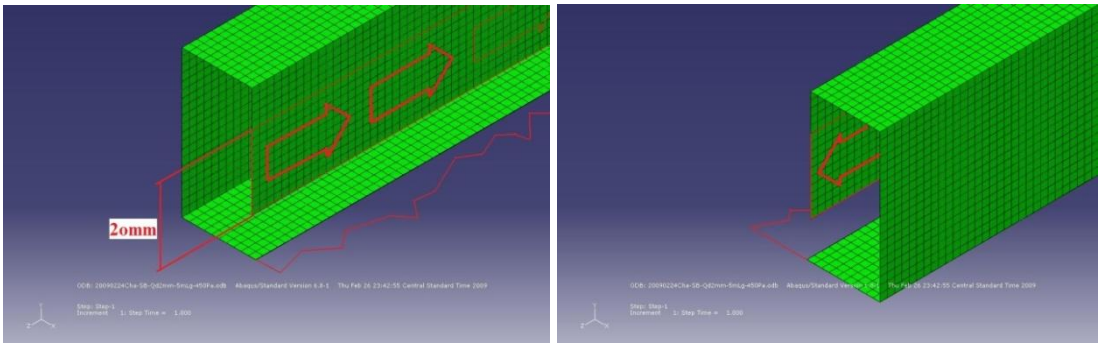

Figure 39. The nastic actuators placed on the split gap flanges produce shear stresses.

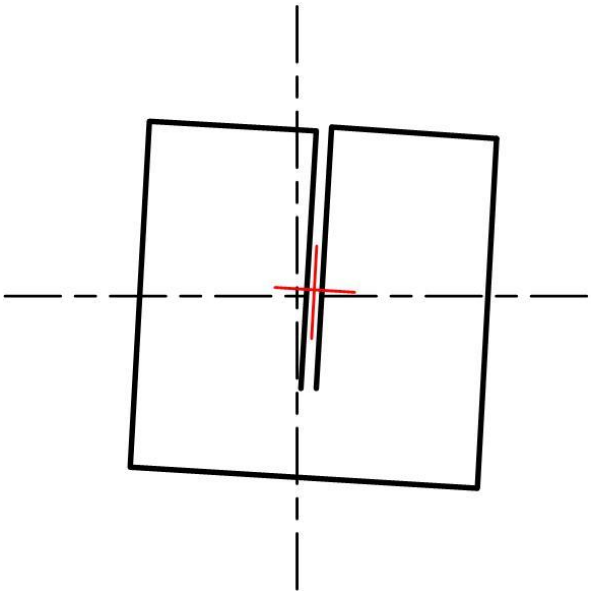

Figure 40. When the nastic material acts on the whole 30mm height, the twist has an eccentric displacement that moves the spar back from its original center.

The spar must produce ±2 degree twisting at its free end. To determine the shear stress that produces this much twist, shear forces were applied using FEA. A ±450Pa shear stress generates 2.11^{o} twist at the free end.

4.2.1.3 Twist Analysis

The spar twist increases with the shear stress. Figure 41 shows the relation between stress and twist. Twist increases linearly with stress and, at 450Pa, the spar twists 2.11 degrees.

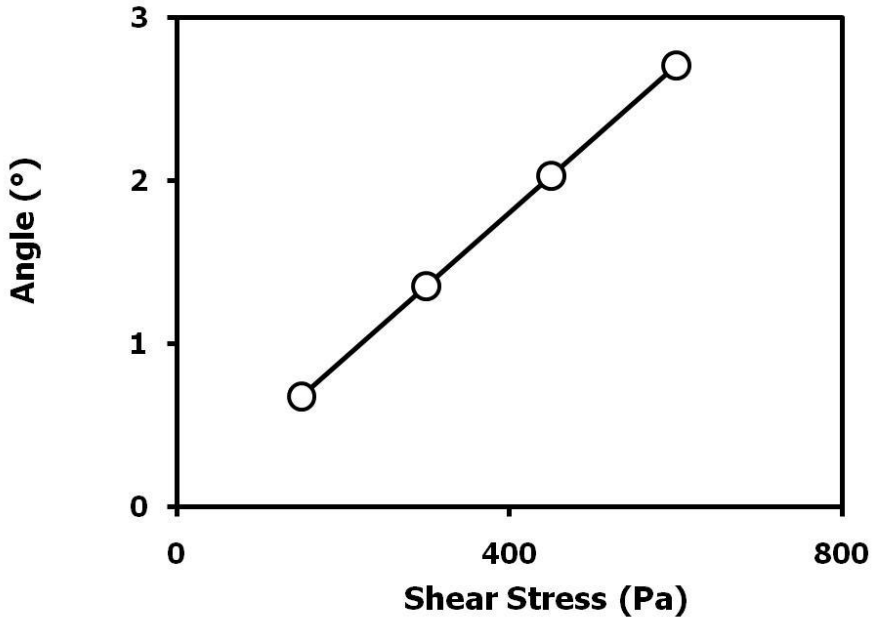

Figure 41. Twisting angle increases with shear stress linearly. When 450Pa is applied, the spar shows about 2 degrees twist.

Twist angle varies along the beam. The spar reaches 2.11 degrees at the free end, but the clamped end condition makes the twist 0 degrees at the beam root. Twist must vary along the beam length. Figure 42 shows the twist distribution. The twists are increase non-linearly near the clamped end, and approach linearity toward the free end. If the spar were longer enough, then the twist would increase linearly.

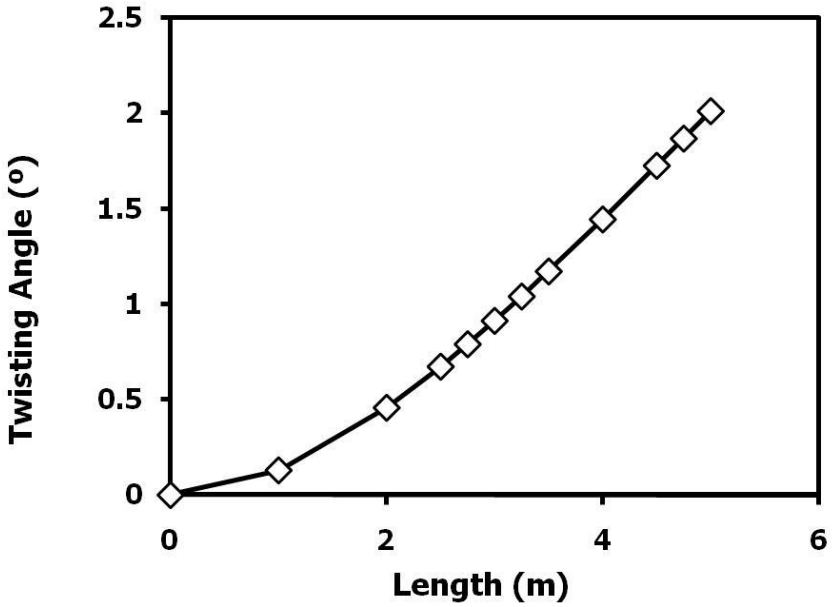

Figure 42. The 450 Pa shear stress increases the twist angle along the spar. At 5m, the spar shows 2 degrees twist.

4.2.2 Prototype Spar Section Locking

The FEA spar is 5m long, but it would be hard to produce that spar for a physical experiment. To verify the FEA results, a prototype spar section was fabricated. Figure 43 shows the spar's dimensions. It is similar to the FEA spar; the length is much shorter,

only 30 cm, and the flanges, 20 mm, are only $\frac{1}{2}$ as deep. Simple tension generated the shear stresses; no nastic material was present.

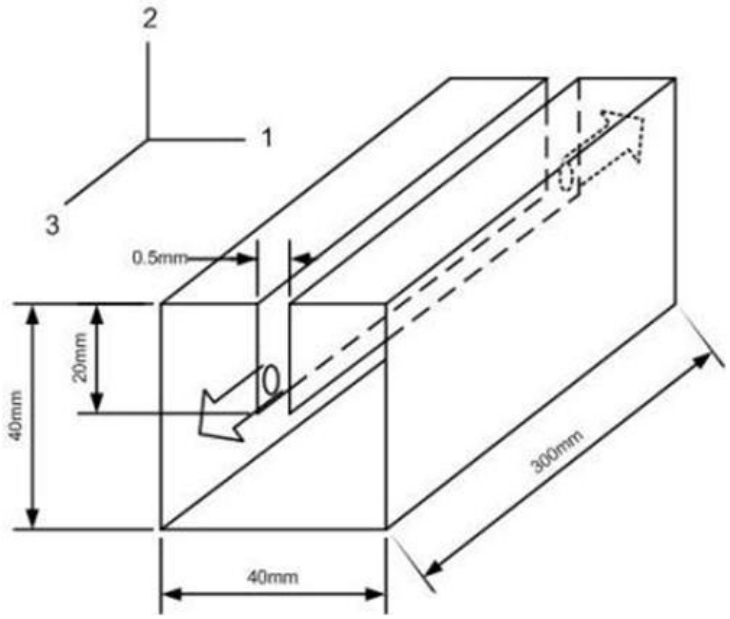

Figure 43. The demonstration spar section has 300mm length, and applying tensile forces on each flange make the spar twist.

Applying tension on each flange twists the spar. As long as plastic deformation does not occur, the spar will spring back when the tension is removed. The spar section's spring constant , K_{al}, can be calculated with below equations.

$$F = K_{al} \times x \qquad K_{al} = \frac{F}{x} \tag{3}$$

where F and x are the forces applied on the flange tabs and the resulting displacement, respectively.

If a locking polymer, for example, Ultem, solidifies between the flanges while the spar is twisted, the polymer has a stress-free state until the actuator stops working. When the tension force is removed, the spar's spring back produces shear stress on the Ultem film. The film resists the stress elastically, and the resistance can be quantified as spring constant. Figure 44 shows how the Ultem film's shear spring constant is defined. The stress applied on the film induces displacement, x, and the ratio, shown as γ (Gamma), between the displacement and specimen thickness.

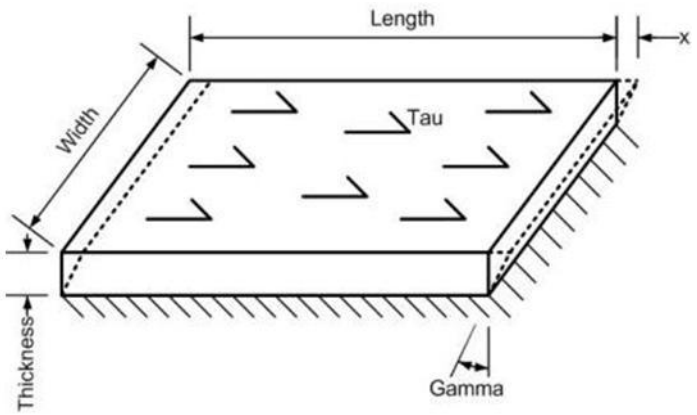

Figure 44. This drawing defines the shear spring constant for a polymer film in simple shear.

The following equations showing how to obtain the shear spring constant for Ultem film. Substituting equation (7) and (8) for (6) eliminates stress term. That the equation (6) put into (5) makes it easy to apply to the spring constant, K, shown in equation (4). The equation (9) shows final equation. This value reflects generic material characteric, so it should not be involved with variable term like a stress.

$$F = K \times x, \qquad K = \frac{F}{x} \tag{4}$$

$$F = \tau \times Area \tag{5}$$

$$\tau = G \times \gamma \tag{6}$$

$$G = \frac{E}{2(1+\nu)} \tag{7}$$

$$\gamma = \frac{x}{t} \tag{8}$$

$$\therefore K = \frac{(E \times Area)}{2(1+\nu)t} \tag{9}$$

The two spring cosntant values from the spar and film determine the locking ratio. If the Ultem's shear spring constant is almost infinite, then the spar will be locked 100% and show no spring back. The other extreme case is that the spar will show no locking at all when the film has small or zero shear spring constant. Figure 45 presents each locking ratio case analyticaly. Case (a) has no embedded locking material, so it will induce 100% spring back. Highly compliant locking material allows the spar spring back approximately 100% in case (b), and an infinitely high spring constant locking material never allows spring back as shown in case (c). When the spar's spring constant equals the locking material's shear spring constant, the force balance produces a 50% spring back like case (d).

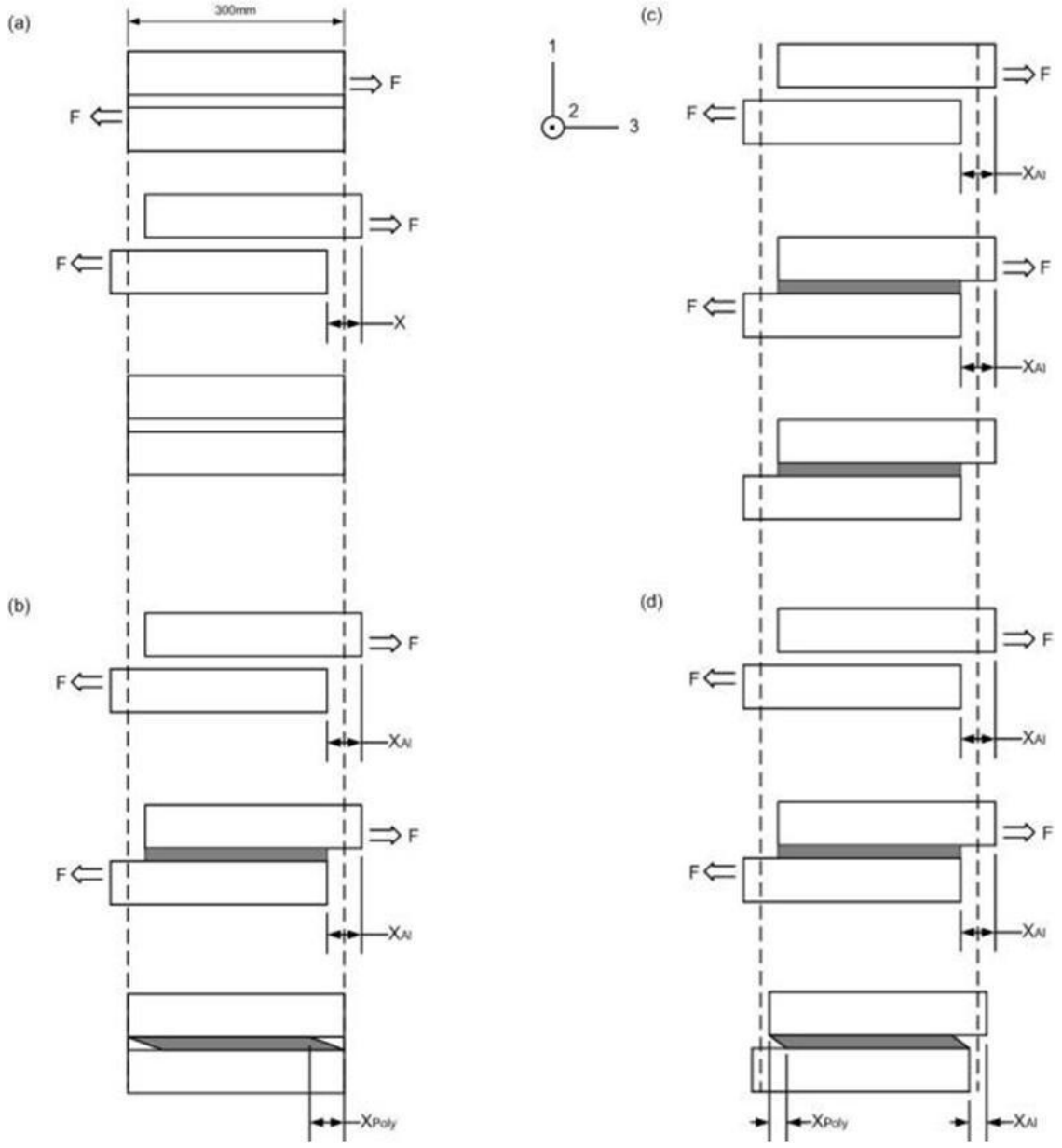

Figure 45. The difference between the spring constants for the aluminum spar and the locking material affects the locking ratio. The spar presents (a) 100% spring back without a locking material (b) approximately 100% spring back with highly compliant locking material (c) 0% spring back with an infinitely high spring constant locking material (d) 50% spring back when the aluminum beam's spring constant equals the locking material's spring constant.

Based on Figure 45 (d), the locking ratio calculation was developed. If the spar spring constant, K_{al}, is equal to the shear spring constant, K_{Poly}, then the displacement in the spar, X_{Al} is balanced with the displacement in the locking material, X_{Poly}, that is 50% locking. Following equations show analytic solution for locking ratio. Equation (10) shows basic spring constant theory in each spar and locking material case. The force in the spar, F_{al}, and locking material, F_{poly}, are the same when the spring back occurs and forces are balanced in the middle. Assume that the spar and film have the same displacement, but the displacements are in opposite directions. With equation (11) substituted into (10), the locking ratio that results is shown in equation (12).

$$K_{al} \times x_{al} = F_{al}, \qquad K_{poly} \times x_{poly} = F_{poly} \quad \textbf{(10)}$$

$$x_{al} + x_{poly} = 1 \quad \textbf{(11)}$$

$$\therefore x_{al}(\%) = \frac{K_{poly}}{K_{al} + K_{poly}} \times 100 \quad \textbf{(12)}$$

The above analytic solution is for the 30 cm spar section's locking ratio. This spar is short and both ends have the same boundary conditions, so the locking ratio can be solved.

Based on the above equations, the locking ratio in this prototype spar section with the Ultem film can be calculated. Substituting following values into equation (9) yields the shear spring constant, K_{poly} : 6.07 GN/m :

- Young's modulus for Ultem film, E : 2.75 GPa
- Film thickness, t : 0.5mm

- Film surface area : $0.01 \times 0.3\ m^2$
- Poisson's ratio for Ultem, ν : 0.36

The section 4.1.1.1 Effective Elastic Modulus, validated the Ultem film Young's modulus value, 2.75 GPa. The spar section spring constant, K_{Al} is 39.72 KN/m that was empirically obtained by spar section calibration in 4.1.2 Spar Spring Constant. Consequently, substitute K_{Al} and K_{poly} into the equation (12). Mathematically, the spar section and Ultem film should not produce spring back. If K_{poly} is much higher than K_{Al} comparatively, then the locking ratio can be almost 1.

As shown in the section 4.1.1.2 Stress Relaxation Test, the Ultem's elastic modulus decreased 20%, 2.20 GN/m, after 10 hours. However, this lowered elastic modulus does not affect locking ratio. The Ultem's shear spring constant at the lower elastic modulus is high enough to lock the section spar.

4.2.3 FEA Verification for Spar Section

The section 4.2.2 Prototype Spar Section Locking, shows analytic results for locking between the spar section and Ultem film. In this section, the result in FEA is proved. Applied forces on the flange tabs twisted the beam and the FEA results provide the twisting angle. Figure 46 exhibits that the angle linearly increases with raising the force.

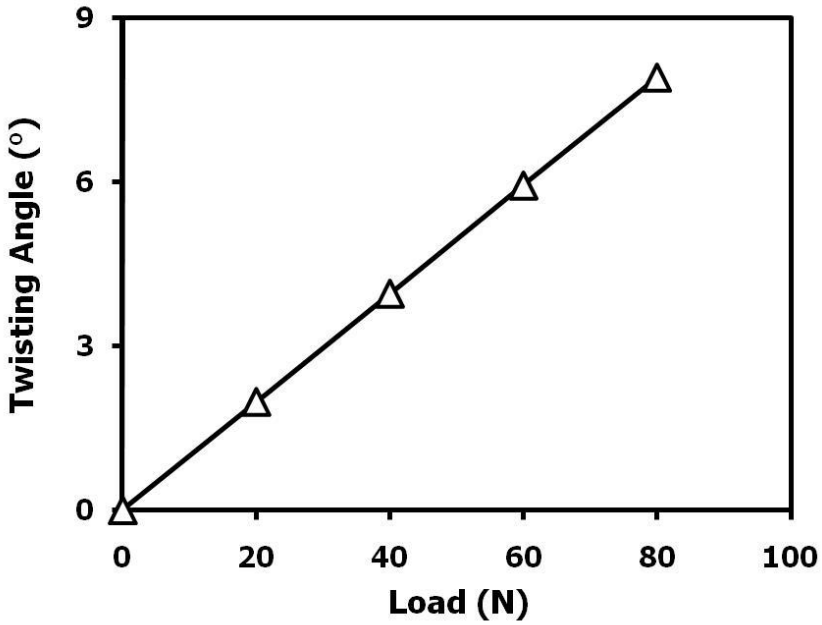

Figure 46. Twisting angle linearly increases with tension in FEA analysis for 30cm long spar.

The prototype spar calibration results shows that applying 2mm displacement produce about 80N. In this FEA, applying 80N on the flange tabs generates 2mm displacement. Thus, the FEA model matches the real model. This 2mm displacement and 80N force applied beam presents 7.91degree twist as shown in Figure 47. This twisting value matches the experimental result. In the section 4.1.2 Spar Spring Constant, spar section applied with 80N produced about 8 degrees twist.

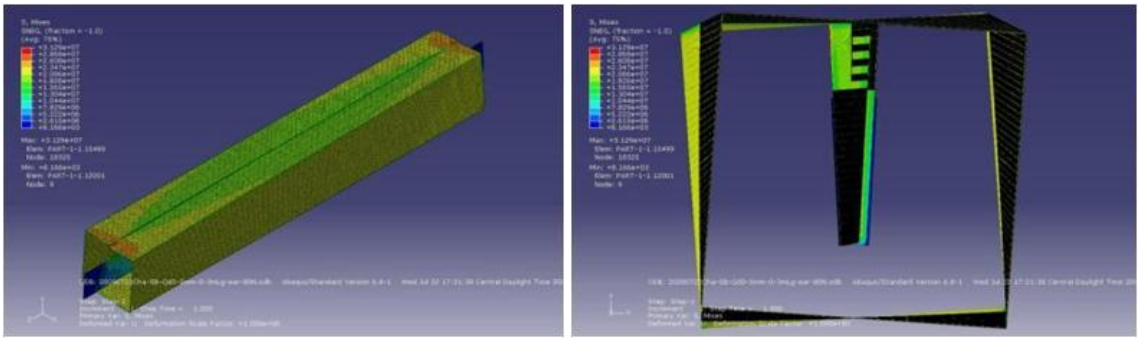

Figure 47. FEA demonstrates 7.91^{o} twist with 80N on the tab.

4.2.4 Analytic Locking Ratio

The boundary conditions for the 5m long spar analyzed by FEA differ from the 30cm spar section 's. The 5 m spar's spring constant is variable because the fixed end stops twist and makes the constant high at the clamped root. The forces and displacements applied through the spar increase from the fixed end to the free end. Figure 48 exhibits the way forces and displacements are obtained. Near the fixed end shown in (a), the length,L1, is small, so the surfaces where shear stresses applied on are small. As shown in (b) and (c), the displacements and forces along the spar increase because the lengths, L2 and L3, are increased.

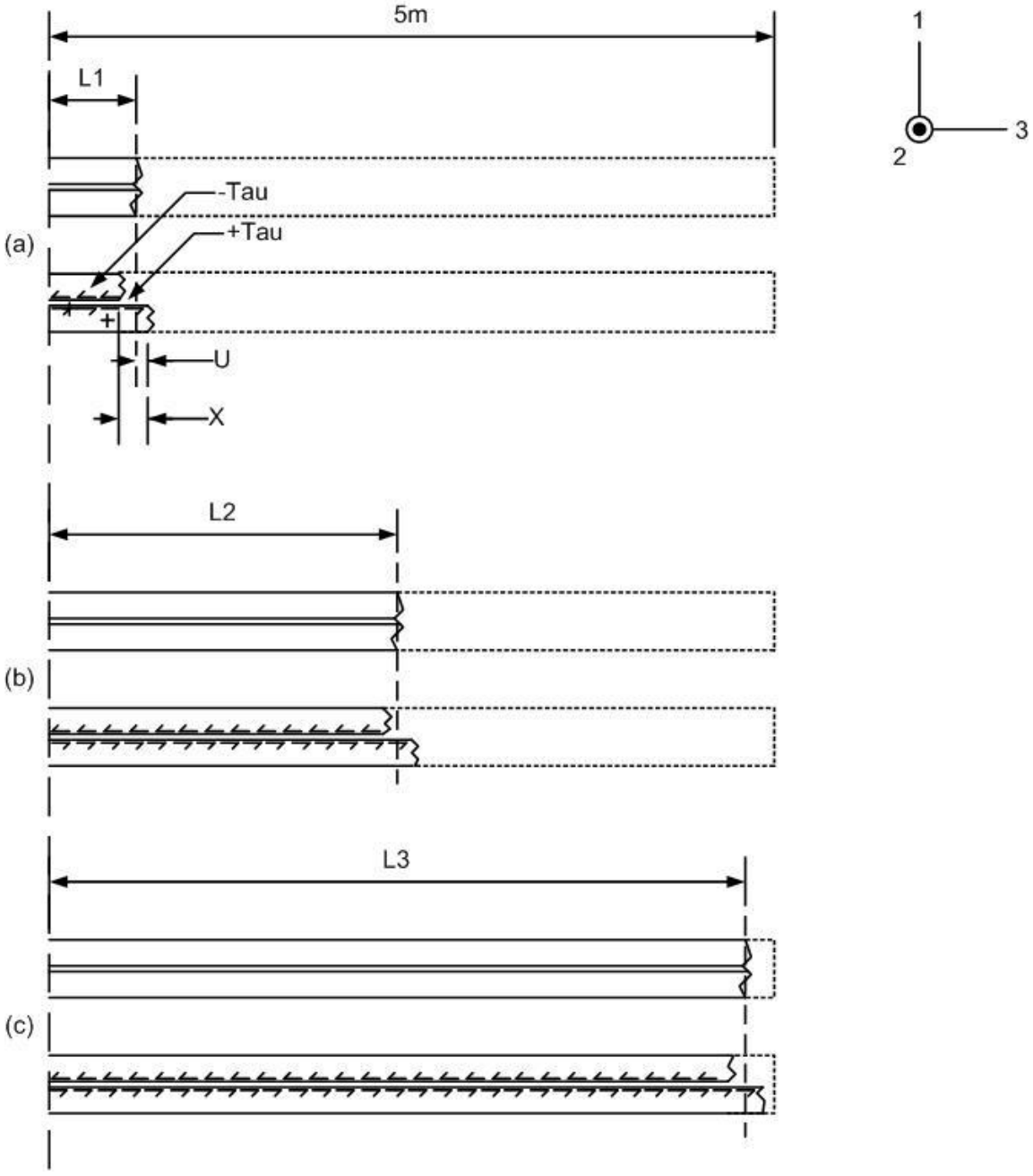

Figure 48. These diagrams show the way obtaining the spring constant for 5m long FEA spar through the length.

An exact spring constant plot might not be possible; the mesh size must be refined near the fixed end. However, twisting does not occur near the fixed end, and the Ultem film does not need to lock the spar in that region.

From equation (5), the force is calculated. The stress is constant, 450Pa, through the spar, but the area is increasing with the spar length. The force acting through the spar appears in Figure 49.

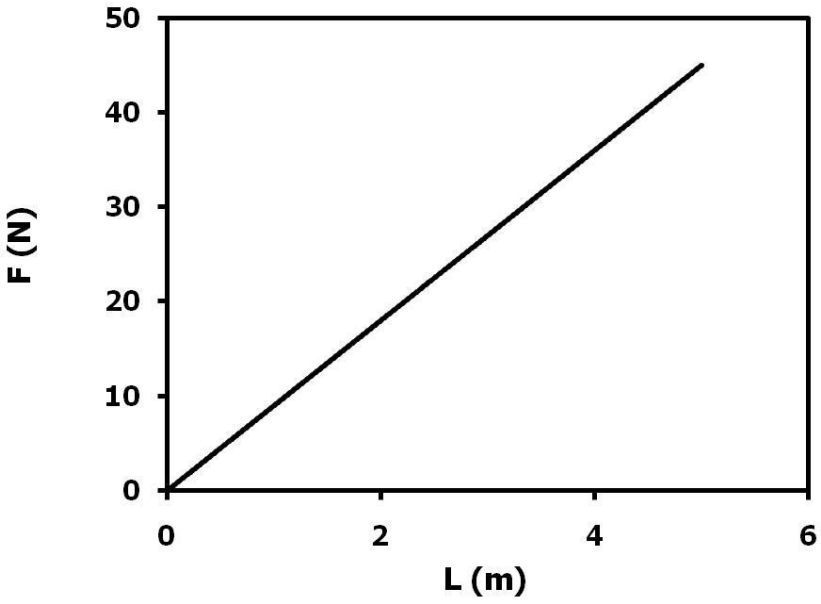

Figure 49. Force is linearly increasing in accordance with growing 5m long FEA spar.

Figure 50 presents 3 direction, i.e., axial, displacement. At the fixed end, the displacement is zero. When the spar is growing as shown in Figure 48, the longitudinal displacement raises toward the free end.

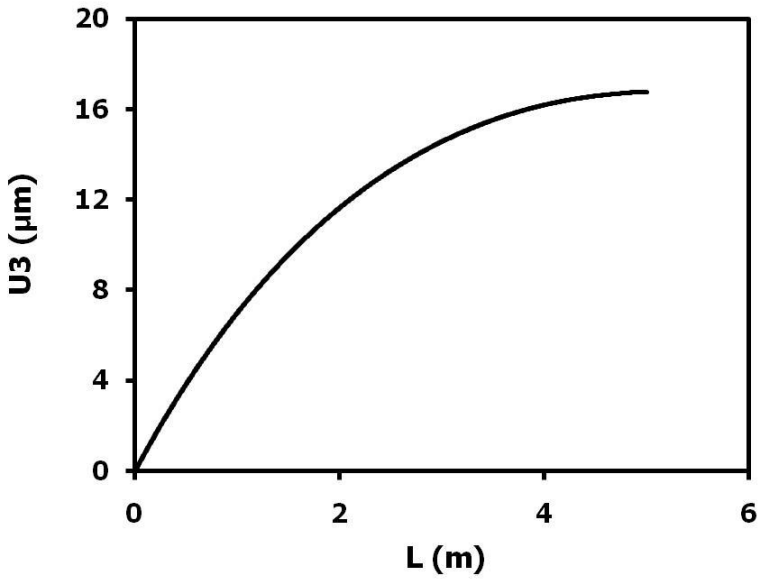

Figure 50. Z direction shows no displacement at fixed end, and nonlinear increase.

Based on simple relationship between the force and displacement in equation (3), the spring constant was calculated. This 5m long spar has variable force and displacement, so the torsional spring constant plot is shown in Figure 51. This constant at the clamped end goes to infinite value because the displacement, denominator in equation (3), goes to zero if the force, numerator, stays constant theoretically. However, the force flowed through this spar is not constant, and also goes to zero near the fixed end as shown in Figure 49. The numerator goes to zero faster than the denominator, so the structural spring constant plot, Figure 51, goes to zero near the fixed end. If fine meshing is used near this end, then the fixed region's spring constant might be different from that presented here.

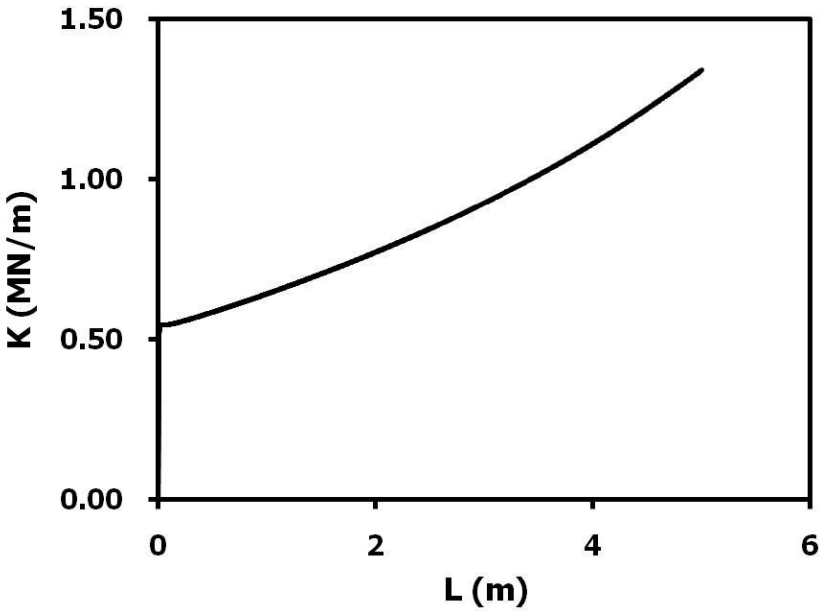

Figure 51. The 5 m spar's spring constant rises along the spar's length.

Near the clamped end, the twist barely occurs, so there is no need to evaluate the locking material performance at the end.

As shown in the equation (9), the Ultem film's shear spring constant is directly proportion to its surface area. When the spring constant is measured while twisting the spar, the film's surface area also increases. The Ultem's elastic modulus, Poisson ratio, and thickness are constant. The area increases linearly with growing the spar. Thus, the shear spring constant plot shows a linear increase as shown in Figure 52.

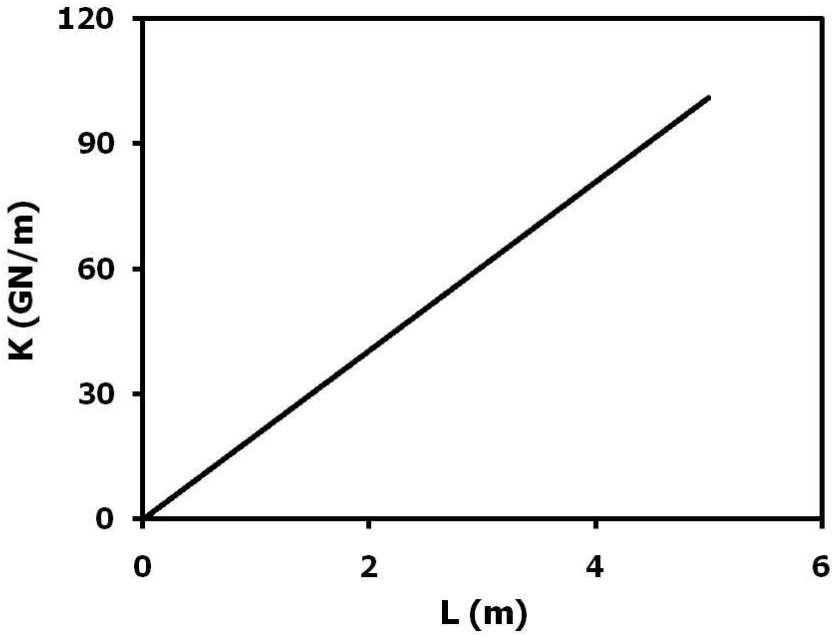

Figure 52. The Ultem film spring constant increases linearly along its length.

The values from Figure 51, the FEA spar structural spring constant, and Figure 52, the Ultem film shear spring constant, substitutes into the equation (12) for locking ratio. Figure 53 exhibits the locking ratio between the 5m long FEA ideal spar and Ultem film. Except last 4mm near the clamped end, the ratio show almost 1, and no spring back occurs.

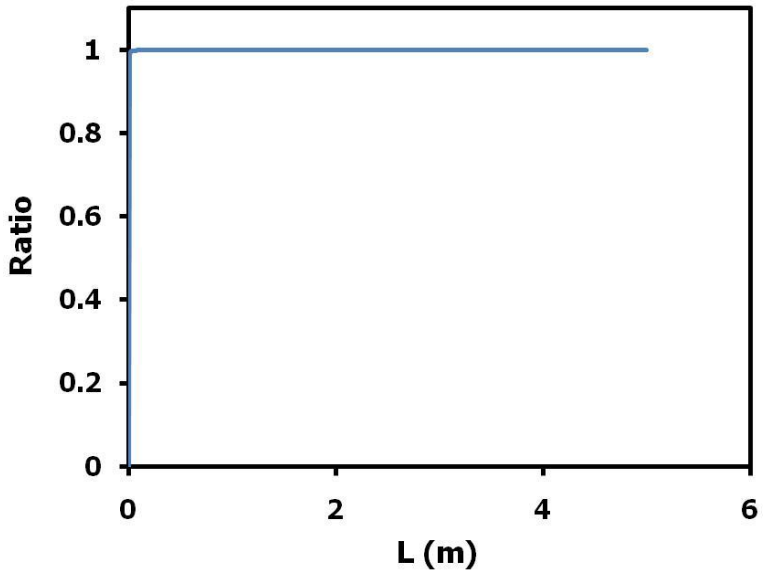

Figure 53. The 5m FEA spar shows almost 100% locking except last 4mm near the fixed end, but the region has practically no twisting because the fixed boundary condition makes the system too stiff. The Ultem film can lock this 5m long spar.

Even the last 4mm shows 99.41% locking in regular 2mm size mesh condition. The biased mesh condition, 0.33mm mesh size, presents 95.69% locking at the last 0.33mm near the clamped end, and 98.49% locking at the last 1.33mm.

In the stress relaxation test, the Ultem's reduced elastic modulus, which is 2.20 GPa, was obtained after 10 hours. In regular 2mm size mesh condition, the locking ratio shows almost 1, and the locking ratio at the last 4mm presents 99.26% with the reduced elastic modulus. The stress relaxation in the Ultem technically does not affect locking ratio.

As mentioned earlier, the fixed end hinders to produce any twists, so the last 4mm does not need locking to maintain twisting. Accordingly, the 0.5mm thick Ultem

film locks the 5m long FEA spar in the twisted state as it did for the prototype spar section according to Figure 53.

Depending on split gap width, the locking ratio can be various. The thickness and shear spring constant in the polymer film have inverse proportion relation as shown in equation (9). If the locking polymer thickness is getting larger, the shear spring constant is getting lower and that reduces locking ratio. Figure 54 depicts various split gap spars and Ultem's locking ratio near the clamped end.

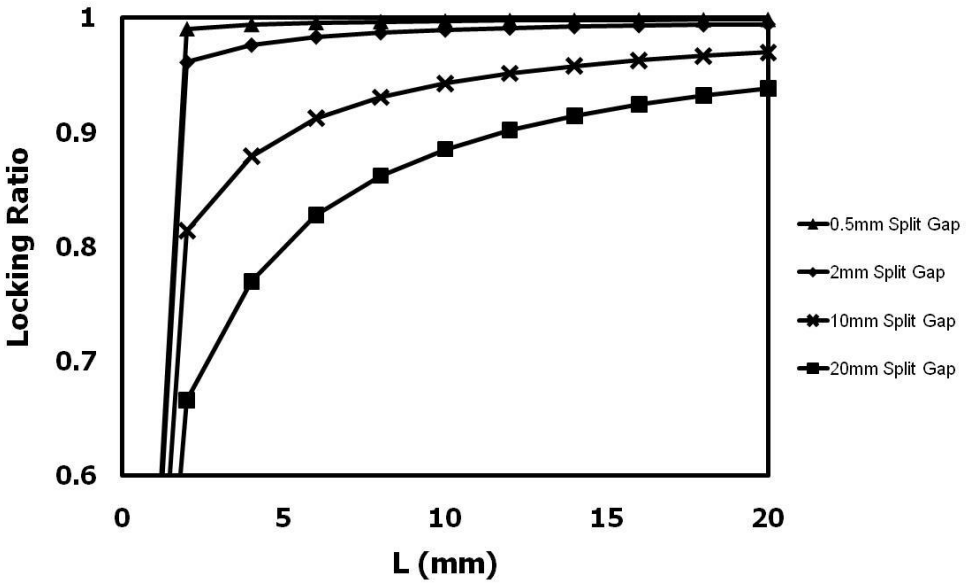

Figure 54. Increasing Ultem thickness and split gap width drops locking ratio.

Thin Ultem and split gap, not only increases locking but also reduces twisting shear force. Figure 55 presents twisting degrees with various split gap widths. It shows the smaller split gap spar produces larger twisting with the same force.

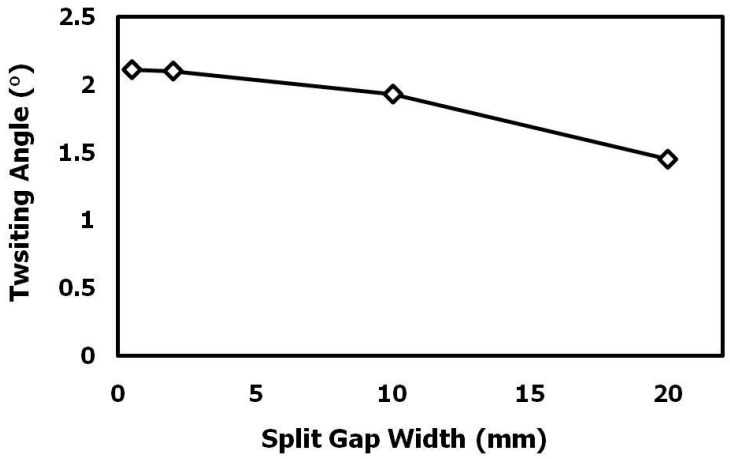

Figure 55. With the same force, wider split gaps produce less twist.

Through the above reason, thin Ultem and thin split gap increases the locking performance and saves the energy when twisting the spar.

5. CONCLUSION AND FUTURE WORKS

5.1 Conclusions

The nastic-material actuated split square spar is locked in the twisted state by a thermoplastic polymer. Even after removing the stresses by actuators, the spar can hold the twisted state. Both the aluminum spar and Ultem film used as the locking material show elastic properties, so the spar spring back may occur after locking the twisted spar and removing actuating forces. In this project, the Ultem film was analyzed to find whether it is able to hold the spring-back force from the aluminum spar, and to determine how much spring-back occurs.

Our design target for the spar is 5m long and 2 degrees twist at the spar's tip. FEA results showed 450 Pa shear stress twists the spar 2 degrees at the tip, and that the Ultem film can lock the spar with almost no spring back. Performing a physical experiment verified this FEA result. A 30cm long prototype spar section was built because fabricating a 5m long spar was not possible. In this spar section, 2mm displacement produced 8 degrees twist. Applying 288^{o}C (550^{o}F) heat during 15 minutes in an electric oven softened the Ultem film without annealing aluminum spar. Cooling process solidified the Ultem, and locked the spring back force. As same as the analytic solution, the spar has no spring back observed in the physical experiment.

Several tests for obtaining the Ultem properties were performed. Stress relaxation test results presented the Ultem dropped applied loads about 20% in 10 hours. It seems

the spar twist will decrease with time. However, the 20% elastic modulus reduction did not affect locking. Tensile test provided elastic modulus that is crucial for attaining a shear spring constant. The result, 2.75GPa, is good enough for lock the spar. Single lap-shear tests showed the solidified Ultem film can bond to aluminum. Depending on the bonding conditions, the stiffness can vary.

Consequently, the 0.5mm thick Ultem film successfully locked both 5m long split square spar in the FEA and the 30cm prototype spar section in the physical experiment.

5.2 Applications

One possible application is a novel aero-vehicle wing. As depicted in Figure 56 (a), the spar is used as the main structure and runs through the air foil's center. The nastic materials provide quick shape change during the operation. This shape changing, shown in (b) and (c), controls angle-of-attack.

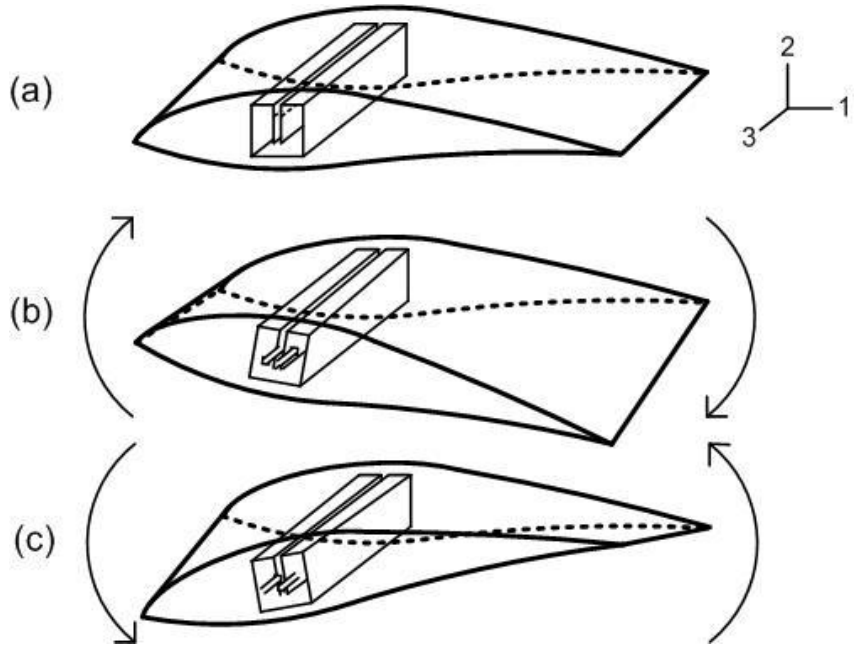

Figure 56. Split spar controls the airfoil.

5.3 Future Complementary Works

Through this research, it is apparent that this locking concept needs complementary work for the real world application. Heating possibly degrades the Ultem. Meshing near the clamped end affects structural spring constant. 5m long spar with a locking material in the FEA model.

5.3.1 ULTEM Degradation

Augh and Gillespie [24] show that Ultem always degrades when heated. In any atmosphere--even in vacuum--the Ultem’s color changes from yellow to black, and the

polymer will crosslink, which destroys its thermoplastic function. Other, stable thermoplastics or lower temperature thermoplastics must be found to lock a twisting beam. The new polymer should provide a locking effect for 10s to 1000s of cycles.

5.3.2 Creep Test

In stress relaxation test, the crosshead holds some strain, and observes a load drop. Creep test demonstrates variable displacement when the tensile test machine holds a load. This research showed stress relaxation test results that indicated dropping the locked spar stiffness relying on time. The stress relaxation and creep test results guide decisions about how much stress the actuators must have to keep the spar stiff, or how the twist will drop with time during a flight.

5.3.3 FEA Spar Model with the Locking Material

The 5m long FEA spar model with the locking material was not analyzed because the computational steps were beyond a masters level project. In this research, the locking material has zero elastic modulus as the spar twists, and the problem was solved analytically. With a better computational resource, it might be possible to demonstrate realistic locking ratio between the 5m long FEA spar and the locking polymer.

REFERENCES

[1] Sater, J., and Main, J. "Plants and Mechanical Motion - Nastic Materials at DARPA," *Proc. International Conference on Adaptive Structure Technology*. Bar Harbor, Maine, 2004.

[2] Findlay, G., and Pallaghy, C. "Potassium Chloride in the Motor Tissue of Stylidium," *Australian Journal of Plant Physiology* Vol. 5, 1978, pp. 219-229.

[3] Cadogan, D., Smith, T., Uhelsky, F., and MacKusick, M. "Morphing Inflatable Wing Development for Compact Package Unmanned Aerial Vehicles," *45th AIAA/ASME/ASCE/AHS/ASC Structures, Structural Dynamics and Materials Conference*. Vol. AIAA No. AIAA-2004-1807, Palm Springs, CA, 2004.

[4] Hennern, H. "Stylidium Turbinatum Column Movement." Wikipedia http://en.wikipedia.org/wiki/File:Stylidium_turbinatum_column_movement.png, [retrieved 7 April 2010].

[5] Gary F. Hawkins, T. S. Creasy., T.J. Curtiss, Michael O'Brien, Wallace Pogue, James Thomas, Hubertus F. von Bremen. "Controllable Active Materials via Internally Generated Pressure, Phase I Final Report." Aviation Applied Technology Directorate, U.S. Army Research Development and Engineering Command, RDECOM TR 06-D-52, 2006, pp. 11-18.

[6] U.S. AirForce. "General Dynamics F-111A." Wikipedia http://en.wikipedia.org/wiki/General_Dynamics_F-111, [retrieved 7 April 2010].

[7] Kudva, J., Martin, C., Scherer, L., Jardine, A., McGowan, A., Lake, R., Sendeckyj, G., and Sanders, B. "Overview of the DARPA/AFRL/NASA Smart Wing program." Vol. 3674, 1999, p. 230.

[8] LEE, S. J. "Active, Polymer-Based Composite Material Implementing Simple Shear," Ph.D. Dissertation *Mechanical Engineering*., Texas A&M University, College Station, 2008, p. 215.

[9] Davidson, J., Chwalowski, P., and Lazos, B. "Flight Dynamic Simulation Assessment of a Morphable Hyper-elliptic Cambered Span Winged Configuration," *AIAA Journal* Vol. 5301, 2003, pp. 11-14.

[10] Hetrick, J., Osborn, R., Kota, S., Flick, P., and Paul, D. "Flight Testing of Mission Adaptive Compliant Wing," *Proceedings of 48th AIAA Structures, Structural Dynamics, and Materials Conference*. 2007, pp. 23-26.

[11] Huber, J., Fleck, N., and Ashby, M. "The Selection of Mechanical Actuators Based on Performance Indices," *Proceedings: Mathematical, Physical and Engineering Sciences*, 1997, pp. 2185-2205.

[12] Esmon, C., Pedmale, U., and Liscum, E. "Plant tropisms: providing the power of movement to a sessile organism," *International Journal of Developmental Biology* Vol. 49, No. 5/6, 2005, p. 665.

[13] Giurgiutiu, V., Matthews, L., Leo, D., and Sundaresan, V. "Concepts for Power and Energy Analysis in Nastic Structures," *International Mechanical Engineering Conference and Exposition*. Vol. IMECE2005-82786, Proc. of ASME-IMECE, Orlando, Florida, 2005.

[14] Hill, B., and Findlay, G. "The Power of Movement in Plants: the Role of Osmotic Machines," *Quarterly Reviews of Biophysics* Vol. 14, No. 2, 1981, p. 173.

[15] Taya, M. "Bio-inspired Design of Intelligent Materials," *Smart Structures and Materials 2003: Electroactive Polymer Actuators and Devices (EAPAD)*. Vol. 5051, Proceedings of SPIE, 2003, p. 54.

[16] Forterre, Y., Skotheim, J., Dumais, J., and Mahadevan, L. "How the Venus Flytrap Snaps," *Nature* Vol. 433, No. 7024, 2005, pp. 421-425.

[17] Nolf, M. "Dionaea Muscipula Closing Trap." 27 April 2009 ed., Wikipedia, http://en.wikipedia.org/wiki/Venus_Flytrap, [retrieved 7 April 2010].

[18] Cadogan, D., Graham, W., and Smith, T. "Inflatable and Rigidizable Wings for Unmanned Aerial Vehicles," *AIAA Journal* Vol. 6630, 2003, p. 2003.

[19] Zanasi, L. "Clamp (tool) ". Wikipedia, http://en.wikipedia.org/wiki/Clamp_(tool), [retrieved 7 April 2010].

[20] Stewart, R. "At the Core of Lightweight Composites," *Reinforced Plastics* Vol. 53, No. 4, 2009, pp. 30-35.

[21] NEUROtiker. "Structure of Polyetherimide." Wikipedia, http://en.wikipedia.org/wiki/File:Polyetherimid.svg, [retrieved 7 April 2010].

[22] "ULTEM PEI." Port Plastics, http://www.portplastics.com/download/pdf/plastics/highPerformance/highPerformance20.pdf, 2004.

[23] TexLoc. "ULTEM Detailed Properties ". Parker-TexLoc, http://www.texloc.com/closet/cl_ultem_properties.htm, 2008.

[24] Augh, L., and Gillespie, J. "Degradation of Continuous Carbon Fiber Reinforced Polyetherimide Composites During Induction Heating," *Journal of Thermoplastic Composite Materials* Vol. 14, No. 2, 2001, p. 96.

[25] ASM International. "Metals Handbook," *Properties and Selection: Nonferrous Alloys and Special-Purpose Materials*. 10th Ed. ed., 1990.

[26] Rswarbrick. "Adhesive." Wikipedia, http://en.wikipedia.org/wiki/Adhesive, [retrieved 7 April 2010].

VITA

Name: Gene Cha

Address: c/o Dr. T. S. Creasy, Department of Mechanical Engineering, Texas A&M University, 309 Engineering/Physics Building, College Statioion, TX 77843-3123.

Email Address: genecha@gmail.com

Education: B.S., Mechanical Engineering, Kyung Hee University, Gyeonggi, Korea, 2006

M.S., Mechanical Engineering, Texas A&M University, College Station, Texas, 2010